A STEP TOWARDS QUANTITATIVE LIPOPROTEIN DENSITY PROFILING ANALYSIS: APPLIED RAYLEIGH SCATTERING

A Thesis

by

MICHAEL NOWLIN

Submitted to the Office of Graduate Studies of
Texas A&M University
in partial fulfillment of the requirements for the degree of

MASTER OF SCIENCE

December 2006

Major Subject: Chemistry

A STEP TOWARDS QUANTITATIVE

LIPOPROTEIN DENSITY PROFILING ANALYSIS:

APPLIED RAYLEIGH SCATTERING

A Thesis

by

MICHAEL NOWLIN

Submitted to the Office of Graduate Studies
of Texas A&M University
in partial fulfillment of the requirements for the degree of

MASTER OF SCIENCE

Approved by:

Chair of Committee,	Ronald D. Macfarlane
Committee Members,	Manuel P. Soriaga
	Stephen B. Smith
Head of Department,	Emile E. Schweikert

December 2006

Major Subject: Chemistry

ABSTRACT

A Step Towards Quantitative Lipoprotein Density Profiling Analysis:

Applied Rayleigh Scattering. (December 2006)

Michael Nowlin, B.A., Coker College

Chair of Advisory Committee: Dr. Ronald D. Macfarlane

Ultracentrifugation and imaging techniques of human blood serum are precise and information-rich methods for obtaining information about an individual's lipoprotein particle content. The information derived from lipoprotein separations via an ultracentrifuge plays a key role in the area of preventative medicine in regards to atherosclerosis. Two of the most critical lipoprotein characteristics, diameter and density, are well preserved with the proper isopycnic gradient. Currently, lipoprotein particles are stained, ultracentrifuged, and profiled through image analysis. This particular technique is helpful in determining particle density and can be correlated loosely with particle concentration. The need to completely quantify lipoprotein concentrations is imperative in assessing risk factors accurately.

Light scattering techniques, primarily Rayleigh scattering, are applied to density separated serum samples in resulting in improved qualitative data with progress in quantitative measurements through imaging alone. The Rayleigh theory dictates that a particle's scattered intensity is based upon the incident intensity, the particle's diameter, and the particle's concentration when strict criteria are met within the sample and imaging apparatus. Applying this innovative imaging technique of Rayleigh scattering to

ultracentrifuge tubes containing separated lipoproteins, particle concentrations at differing diameters can be calculated.

This thesis primarily goes through the time consuming task of optimizing the innovative Rayleigh scattering system so that correct quantitative estimations can be performed. Constrained by Rayleigh theory and system limitations, lipoproteins of 15 nm to 35 nm are focused upon. By doing so, previously disguised data in regards to lipoprotein subclasses is exposed. Lipoprotein diameters are estimated from Rayleigh imaged serum profiles and the estimations are confirmed through secondary size analysis achieved by dynamic light scattering instrumentation. In addition to Rayleigh optimization, a strategy for quantifying the ultracentrifuged lipoprotein particles using the recently applied scattering technique is explained in detail providing a foundation for further research. In regards to all feasibility studies presented within this thesis, much success was achieved in furthering quantitation efforts in lipoprotein density profiling.

ACKNOWLEDGEMENTS

I would like to extend my thanks to Dr. Ronald D. Macfarlane for allowing me the opportunity to conduct independent graduate level research. By instilling a very arduous schedule of teaching, academics, and experimentation, I was able to develop confidence in an analytical laboratory.

A special thanks is extended to Dr. Rosemary Walzem for allowing me to conduct an important portion of my research in her laboratory. Without her leniency and kindness, the last leg of my research would have been much more demanding.

This research would not have been possible without the collaborative efforts of Scott & White Hospital. This work was funded by the NIH Heart and Lung and Blood Institute.

TABLE OF CONTENTS

Page

LIST OF FIGURES

FIGURE Page

FIGURE Page

LIST OF TABLES

INTRODUCTION

In today's society, mortality is affected by numerous ailments, terminal illnesses, acts of Mother Nature, and catastrophic accidents that can occur anywhere on a daily basis. In the eyes of any natural hero, a perfect society would be able to cure and prevent all such situations affecting one's mortality. However, with the overwhelming number of ailments in the world, it is probably wisest to develop preventative measures that will stop health disorders before they ever become a problem. For instance, cardiovascular diseases (CVD) are an ailment that affects more than 71 million Americans according to the American Heart Association's Heart Disease and Stroke Statistics of 2003. Essentially one in every three adults has some form of CVD, and 38 percent of all American deaths in 2003 were a result of the disease [1].

CVD is actually an enveloping term as numerous diseases concerning the entire cardiovascular system fit in the classification. A CVD that has topped the statistical charts of mortality in America for decades is coronary heart disease (CHD). Although it has recently been displaced from the top position, coronary heart disease still requires a huge effort in continuing its decline from the mortality charts. Coronary heart disease, also known as coronary artery disease, is a narrowing of the small blood vessels and coronary arteries that supply blood and oxygen to the heart. The narrowing of the coronary arteries due to the condition in which fatty material is deposited along the walls of arteries developing atheromas is better known as atherosclerosis. This fatty material thickens, hardens, and may eventually block the arteries.

This thesis follows the style of *Analytical Biochemistry.*

Atherosclerosis is often referred to as an inflammatory disorder that is initiated by a variety of factors. Thankfully, for the medical world this disease is preventable through awareness and understanding the risk factors associated with it. Causes attached to the disorder include genetic high blood pressure, heavy use of physical irritants like nicotine, other cardiovascular diseases like diabetes, and cholesterol synthesis. In addition to the likely causes of the disorder, the medical community has connected certain physiological risk factors allowing individuals to prevent and slow the progression of the disorder.

Atherosclerosis

Atherosclerosis is known to affect both medium-sized and large-sized arteries of the brain, heart, kidneys, other vital organs, and legs. There are two main theories about why atherosclerosis develops. First, high levels of cholesterol in the blood injure the artery's lining, causing an inflammatory reaction and enabling cholesterol and other fatty materials to accumulate forming atheromas [2]. Secondly, repeated injury to the artery's wall, known as denudation, may occur through various mechanisms involving the immune system, direct toxicity, and altered blood flow through elevated blood pressure or hypertension. In both cases, there are changes that can lead to the formation of atheromas. The two theories are probably interrelated and are not mutually exclusive.

Whether the lesions are a resultant from endothelial dysfunction or just endothelial denudation, the inflammatory response and promotion of atherosclerosis is relatively identical. In figure one, the main stages of inflammatory response to endothelial dysfunction is pictured [3]. The stages, one through three, are pictured from left to right in figure 1.

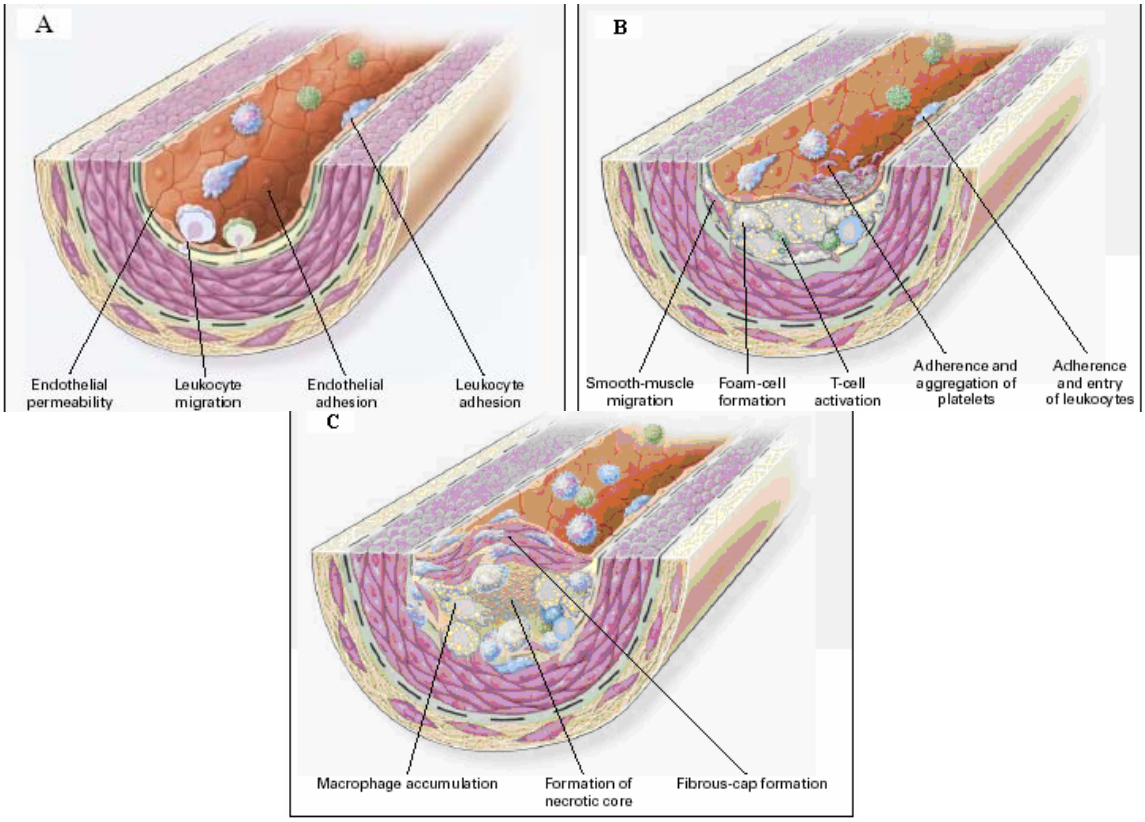

Fig. 1. Progression of formation of atheromas in the vascular system, A through C [3].

The figure depicts the general stages of atherosclerotic formations from once the endothelial dysfunction occurs, to the formation of large atheromas. Initially, the endothelial cells over-express adhesion molecules (VCAM-1 and ICAM-1) in response to the injured portion [4]. These adhesion molecules then lay the foundation for the inflammatory cascade [5]. Platelets are attracted to the injured areas releasing prostaglandins which in turn promote endothelial cell growth at the expense of making porous sections in the wall. The increased porosity of the endothelium enhances the permeability to plasma lipoproteins traveling through the vascular system and increases the adhesiveness for blood leucocytes, monocytes and T-cells. Monocytes adhere to the

endothelium and our allowed to migrate through the endothelium and basement membrane [4]. Activation of monocytes and T cells leads to up-regulation of receptors and scavenger receptors on their surfaces [3].

At this point, the extra traffic developing in the subintimal space causes excess retention of low density lipoproteins (LDL) making them vulnerable to Apo-B100 oxidation by free radicals. The oxidized LDL particles are then attacked by the monocytes and macrophages as the scavenger receptor allows their uptake. Upon uptake, the vast amounts of cholesterol contained by the LDL particle are deposited causing monocyte growth. The uptake of the oxidized LDL through the scavenger receptors does not have any negative feedback; large amounts of oxidized LDL can be incorporated into the macrophages resulting in a foam cell [6,7]. As macrophages grow in the subintimal space, smooth muscle cells will eventually respond by migrating throughout and on top of the enlargement to restore the elasticity of the artery. This cycle can be repeated numerous times until the artery becomes hardened and clogged impeding the flow of any blood.

Although wide-ranging, this overview is informative on the development of atheromas during the progression of atherosclerosis. The importance of low density lipoproteins was mentioned in the deposition of cholesterol escalating the formation of foam cells. However, LDL particles are not the only abundant lipoproteins in circulation, nor are they the only lipoproteins that contribute to atherosclerosis. The entire scope of lipoprotein metabolism and transport dictates the amount of atherosclerotic lipids present in an individual. Analysis of lipoproteins in one's serum can also offer the researcher a window to prominent risk factors of atherosclerosis.

Lipoproteins

The transportation of cholesterol, cholesterol esters, and triglycerides in blood plasma is an intensely studied area in medicine. The nanoparticle sized packages responsible for the transport are better known as lipoproteins. Lipoproteins are essential to the understanding and prevention of cardiovascular related diseases as their proportions contained within the blood can allude to a number of risk factors. Figure 2 depicts the general structure of a lipoprotein particle. The size and the type of proteins contained by the particle are its defining characteristics.

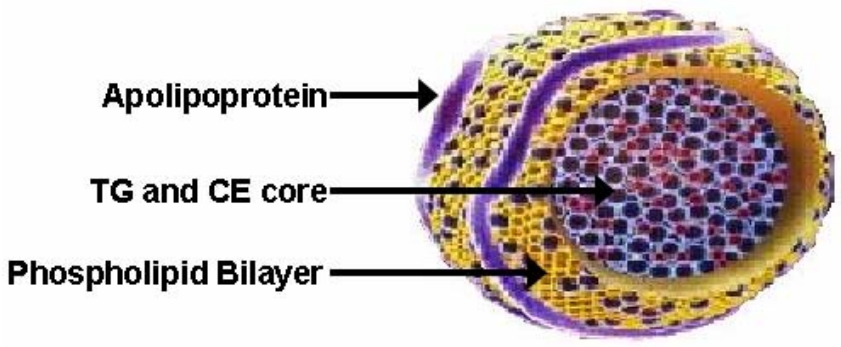

Fig. 2. General structure of a serum lipoprotein particle.

The surface of the lipoprotein particle contains an amphiphatic phospholipid bilayer, non-etserified cholesterols, and most importantly the defining constituent, apolipoproteins [8]. The hydrophobic core of the particle consists of cholesterol esters and triglycerides. The apolipoproteins attached to the surface of the particle dictate the particle's role in lipid transport throughout the body. The apolipoproteins are solely

responsible for interacting with numerous protein receptors within the body as lipid content is distributed or up taken. Differences in apolipoprotein content as well as core lipid content allow classification based upon physical characteristics. The following table sums up the very general classifications of lipoprotein particles.

Table 1. Classification of lipoproteins [8].

Lipoprotein	***Density (kg/L)***	***Particle Diameter***	***Apolipoprotein***	***Function***
Chylomicron	<0.95	80-1200 nm	Apo B-48, A-I, A-II, A-IV, Apo C, Apo E	Triglyceride carrier
VLDL	0.95-1.006	30-80 nm	Apo B-100, A-I, A-II, A-IV, Apo C, Apo E	Triglyceride carrier
IDL	1.006-1.019	26-35 nm	Apo B-100, Apo E	Triglyceride carrier
LDL	1.019-1.063	15-26 nm	Apo B-100	Cholesterol carrier
Lp(a)	1.050-1.100	25-35 nm	Apo B-100, Apo(a)	Undetermined
HDL	1.063-1.21	5-12 nm	A-I, A-II, A-IV, Apo C, ApoE	Cholesterol removal

The main classes of lipoproteins are easily identified and confirmed through separation by ultracentrifugation. However, further subspecies of the lipoprotein classes are present and they are distributed throughout their respective classification. Through further analysis, many subspecies have been determined and related to particular risk factors of CVD. Primarily the small dense subspecies of the LDL class as well as the

Lp(a) class have gotten the most attention as being prominent risk factors in regards to atherosclerosis.

Low Density Lipoprotein Classification

In a study conducted by Rafael Carmena, it is reported that "elevated LDL-cholesterol levels are associated with a risk of CHD, and LDL cholesterol continues to be the primary target of therapy and prevention" [9]. Because of numerous corroborating studies of this sort, LDL cholesterol has been given the moniker, "bad cholesterol".

The LDL particle's surface mainly consists of a phospholipid bilayer and the apolipoprotein molecule, Apo B-100. The core consists largely of cholesterol esters and has the highest ratio of cholesterol ester to lipids than any other lipoprotein particle. Cholesterol ester is the form of cholesterol that is stored by cells for later use. The LDL particle is a result of numerous interactions between very low density lipoprotein (VLDL) particles and lipoprotein lipase. After successive interactions, the VLDL particle loses its triglyceride content and surface apolipoproteins until the denser, cholesterol ester laden LDL particle remains [10]. This particle has a half life of 2-2.5 days in circulation giving it ample opportunity to deposit cholesterol through out the body [10]. Although the liver normally disposes of this particle through circulation, numerous cells contain very specific LDL receptors offering specific binding and internalization of this particle.

The LDL receptor has specificity for the Apo B-100 protein present on the surface of the LDL particle. Once bound, the particle is internalized by the cell in an endocytotic vesicle that combines with a primary or preexisting lysosome (see figure 3). The low

density lipoprotein is further degraded as the protein itself is cleaved of amino acids and the cholesterol ester is hydrolyzed by a lysosomal acid cholesterol ester hydrolase [11].

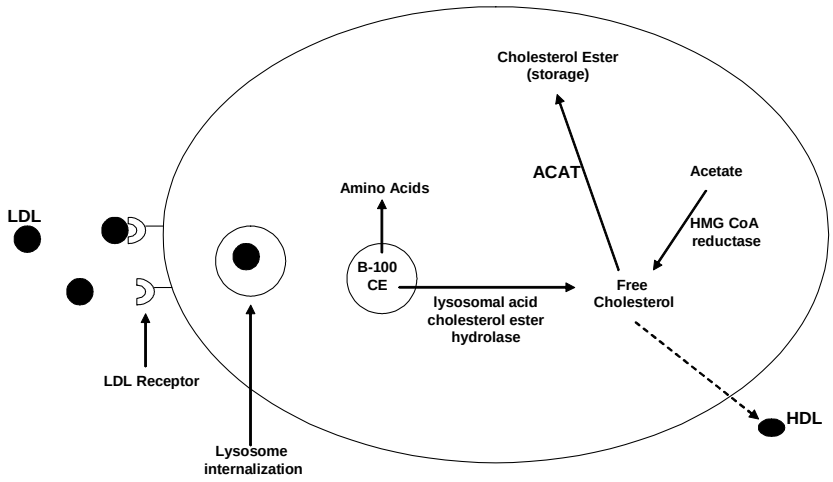

Fig. 3. Overview of LDL metabolism [10,11]

The free cholesterol can stimulate the production of cholesterol esters for storage purposes through the activation of membrane bound fatty acyl-CoA: cholesterol acyltransferase (ACAT) [12]. In addition to this, the recently abundant amount of free cholesterol will also suppress the synthesis of cellular cholesterol by impeding the activity of 3-hydroxy-3-methylglutaryl coenzyme A reductase (HMG-CoA reductase) [12]. Once the LDL contents are degraded and allocated, excess cellular cholesterol can be transported away and back to the liver by means of the high density lipoprotein particle. Due to the cycle of LDL depositing cholesterol in the cells and HDL removing

excess cholesterol from cells, the association of "bad cholesterol" and "good cholesterol" has been deemed respectively.

With knowledge of the simple lipoprotein transport system, one can see how certain lipoproteins have a more vital role in the occurrence of atherosclerosis. By separating one's blood serum into its separate lipoprotein fractions, one can tell a great deal about the individual's health. However, basic LDL concentration determinations can not solely be used for risk assessment of atherosclerosis since the heterogeneity of the LDL particle classification has recently demanded attention.

Low Density Lipoprotein Subclasses

Low density lipoprotein particles get much attention as they are known to be the bearers of "bad cholesterol," but current research has gone beyond the overall scope of the LDL particle as heterogeneity haunts this class. It is postulated that certain subclasses of LDL predict atherosclerosis most effectively. The general public has always been assumed to have monodispersed LDL particles, but overwhelming evidence counters this thought by dictating that general public depicts polydispersity of LDL particles to some degree.

Most published accounts state that LDL subfractions are typically split into two groups. LDL subclass phenotype A is characterized by a predominance of large LDL particles (>25 nm), whereas LDL subclass phenotype B is characterized by a predominance of small LDL particles (<25 nm) [9]. It has been established that the confirmation of the Apo B-100 protein is distinct between LDL subclasses contributing to the differences in their atherogeneity [13]. Supposedly, the conformational changes of

the surface protein in the small dense LDL portions allow the particles to resist binding to the LDL receptor, leading to high susceptibility of subendothelial oxidation due to prolonged subendothelial residence [14]. For this reason, the small dense portion of LDL particles is highly associated with atherosclerosis.

In more recent accounts, the existence of multiple subclasses of LDL characterized by variations in the known physical and chemical composition has been widely recognized [15]. The newly recognized classes include both LDL phenotypes, but they go well beyond just two subclasses. Table 2 is a quick summary of the common subclasses of LDL. The three subclasses listed are the most general of the subclasses, but other publications have been known to separate these subclasses even further. For example, Sonja Alabakovska splits phenotype A into two additional subclasses leading to a total of 4 LDL subclasses while Paul T. Williams identifies up to seven subclasses [16,17].

Table 2. Classification of human plasma LDL subclasses [16,18].

Dominant LDL Subclass	***Phenotype***	***Density (kg/L)***	***Particle Diameter***	***Function***
LDL	A - B	1.019-1.063	17-27 nm	Triglyceride Carrier
LDL I	A	1.020-1.034	24 - 26 nm	Inversely related to plasma TG and CHD risk
LDL II	B	1.034-1.044	22 - 24 nm	Principal carrier of cholesterol esters, most abundant LDL subclass
LDL III	B	1.044-1.060	18 - 22 nm	Positively associated with plasma TG and CHD risk

In 2003 the National Cholesterol Education Program stated that elevated levels of small dense LDL of phenotype B was an accepted emerging cardiovascular risk factor [19]. Although genetic predisposition plays an integral role in the accumulation of phenotype B, it has also been proven that environmental factors such as a diet high in fat can lead to elevated levels of small dense LDL [20]. However, the presence of small dense LDL has yet to be independently associated with atherosclerosis in a clinical setting. Typically, when small dense LDL is present, other risk factors associated with atherosclerosis will be present [21].

Until recently, flotation rate, sedimentation rate, or sedimentation equilibrium separations were the means by which the major classes of lipoproteins would be separated. Excision of the class fractions and further analysis would provide information on the subclasses present. Novel density gradients produced in our laboratory allow particular lipoprotein classes to be separated at a much more broadened and gradual rate so that subclasses can be potentially detected without further analysis.

Lipoprotein(a)

Lipoprotein(a) is another Apo B-100 based lipoprotein that is highly associated with atherosclerosis. Although the particle is associated with cardiovascular disease, little is actually known about its function and role in the disease. Fortunately, there are a few unique characteristics about this lipoprotein that makes it a good detectable marker within isopycnic separation and imaging procedures.

Lp(a) is an LDL like particle as its surface consists of a Apo B-100 molecule and cholesterol ester core of up to 45 percent [22]. The unique aspect of this molecule is that

its surface also contains a unique glycoprotein called apolipoprotein(a). Apolipoprotein is covalently attached to the Apo B-100 molecule via a disulfide bond [23]. Apo(a) is highly glycosylated, up to 28%, and because of multiple isoforms its mass varies between 200-800 kDa [8,24] Figure 4 provides a nice indication of what a typical structure of Lp(a) is. K represents the types of Kringles present on the apoprotein. A Kringle is a highly conserved, tri-loop polypeptide structure stabilized by three disulfide bridges [8].

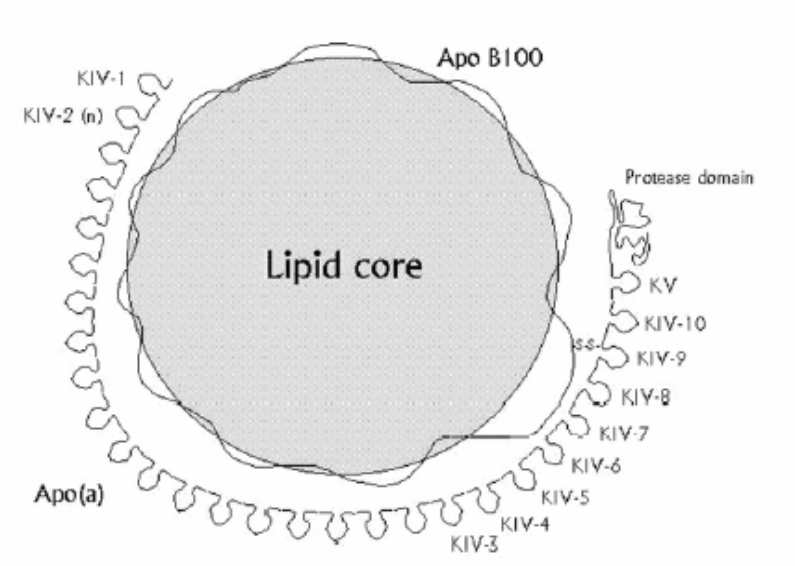

Fig. 4. Structure of Lp(a) [24].

The LDL core of the Lp(a) particle is approximately 25 nm and depending on the glycosylation and mass of the apolipoprotein(a) portion, the size of this particle can vary from 25 nm up to 35 nm [8]. The truly intriguing aspect of this lipoprotein is the fact that it has a respective density in the range of 1.06 and 1.11 g/m [24]. When this data is compared to the overall lipoprotein density information presented on table 1, one can

immediately see that this particle is out of place. What is meant by this is that the particle has a relative density equal to that of HDL particles, but it boasts a particle diameter of nearly three times the size of HDL. This is an important feature for gathering light scattering data on this particle. Reasons to this importance will be explained in the Rayleigh scattering portion of this thesis.

The role of Lp(a) in cardiovascular related diseases has yet to be confirmed as an independent risk factor, but the presence of this molecule in patients with atherosclerotic lesions and advanced symptoms of the disease can not be overlooked. Its athrogeneicity is attributed to its large cholesterol ester core which can be easily deposited into atherosclerotic plaques much like LDL. In addition to this, the apoprotein(a) has proven to be a competitive inhibitor of plasminogen action within the circulatory system [22].

Apolipoprotein(a) can enter the subendothelial area by means of the kringles binding to fibrin or by macrophage cells [25,26]. Fibrin is the main protein component of blood clots and if bound to Lp(a), the fibrin can not be disintegrated allowing clots to assemble. Once inside the subendothelium, the Lp(a) particles will act much like LDL particles as far as susceptibility to oxidation goes. Once oxidized, they will be engulfed through the scavenger receptors on macrophages and will eventually overtake the macrophage. The cholesterol deposited inside the macrophage will ultimately lead to foam cells and fatty streaks within the artery wall.

Currently, detecting Lipoprotein(a) as a risk factor includes immunoassays, chromatography, or a combination of immunoprecipitations and isopycnic ultracentrifugation separations. Isopycnic separations can not be solely used as the density of Lp(a) overlaps with the density of HDL, causing the banding to be a

heterogeneous mixture of Lp(a) and HDL particles. However, the large diameter of the Lp(a) particle lends itself to other detection techniques explained in this thesis. A properly tuned light scattering apparatus should be able to detect the Lp(a) particle that is supposedly hidden within the HDL band of an isopycnic separation.

Ultracentrifugation

Analytical ultracentrifugation is the most widely used research technique within the biology and biochemistry realm. A centrifuge uses centrifugal force (g-force) to isolate suspended particles from their surrounding medium due to differing sedimentation rates. Applications for centrifugation are vast and may include separation of organelles, sedimentation of cells and viruses, and isolation of macromolecules such as DNA, proteins, or lipoproteins. The two main groups of centrifugation used in these applications are known as rate separations or isopycnic separations.

Rate separations permit particles to either float (sequential flotation) or sediment (rate-zonal sedimentation) through a density gradient at differing velocities depending on the physical characteristics of the particle. Physical characteristics may include, size, shape, viscosity, charge, and mainly the density. This type of separation is always conducted in a heterogeneous environment with the sample being layered on top of or underneath a gradient of differing density [27].

An isopycnic separation is defined as a particle sinking/sedimenting through a medium until it reaches a position where the density of both the medium and the particle are identical. A gradient solvent is mixed with the sample creating a homogeneous solution prior to centrifugation. Typically, the chosen gradient consists of a low molar

concentration salt solution that has a known density slope. Manipulation of this gradient can also cause shallow or deep separations depending on the data needed to be extracted. Once the isopycnic points of all the particles contained in the solution are achieved, the location of the particles within the gradient can be compared to the known data on the gradient allowing exact particle densities to be determined. When it comes to separating lipoprotein particles, isopycnic separations via a density are the chosen methods used.

Our laboratory utilizes the isopycnic density gradient separation method. Brian Hosken's 2002 Dissertation outlined the sedimentation theory as well as other mathematical intricacies associated with our method of ultracentrifugation [27]. The factors that influence the time required for lipoproteins to form isopycnic bands are outlined in the following equation.

$$t = \left(\beta^*(\rho_p-\rho_m) / \omega^4 r_p^2 \upsilon\right) * \left(1.26 + \ln\left((r_b- r_t)/\sigma\right)\right) \quad (1)$$

Where t is time in seconds, ρ_p is the density of the particle, ρ_m is the density of the medium, ω is the angular velocity, υ is the velocity of the particle, r_p is the distance that the particle has to travel to reach equilibrium (path length), r_b is the bottom of the gradient in cm, r_t is the top of the gradient in cm, σ is the standard deviation of the distribution, and β is the proportionality constant which is a function of the solute's thermodynamic properties defined as follows [28,29].

$$\beta = RT / M^*(1- \upsilon_s\rho_g) \quad (2)$$

R is the gas constant (8.314×10^7 ergs/mol K), T is the temperature (K), M is the molecular weight of solute, υ_s is the partial specific volume of the hydrated solute, and ρ_g is the density of the gradient. Thankfully, the β proportionality constant does not have to be calculated for each gradient used since a wide variety have already been calculated and published [29].

The equation shows that the most important factors influencing the time required to form isopycnic bands is the speed of the rotor and the distance the particle travels. To achieve a short particle path length a fixed angled rotor is chosen for our applications. A fixed angled rotor does not have the shortest path length when all rotors are considered, but its path length is short and rotors of this sort are able to withstand higher centrifugal forces. In addition to rotor choice, an ultracentrifuge that can reach extreme speeds of up to 120K rpms or more will enable equilibrium banding time to be significantly reduced.

The major downside to analytical isopycnic separations is the fact that rotors are designed for separation efficiencies, not high sample throughput. This means that ultracentrifugation is a research technique only since the throughput of daily samples is very low. It is hypothesized that creating ultracentrifugation tubes of a much smaller size than what is currently produced can increase sample throughput greatly when the common dimensions of UC tubes and rotors are considered. In order for this to take place, feasibility of a much smaller UC tube would have to be proven, and then the machining of new rotors to house the smaller tubes can take place.

Density Gradients

Historically, sucrose has been employed for rate separations as it offers decent banding resolutions in addition to its transparency and extremely low costs [30]. However, the poor resolution, poor reproducibility, and unstable gradient of the sucrose in rate separations beckoned new gradient innovations necessitating extremely high resolution and versatility. To meet the desires of researchers, it was essential to create self forming gradients to be used for isopycnic separations. It has been previously explained that isopycnic separations provide the best band resolution and self forming gradients are the most reproducible types of gradients for isopycnic separations.

Self generating gradients can be easily produced and are very predictable as far as concentration range, time to reach equilibrium, and gradient slope is concerned. Through extensive research it has been determined that the greatest densities in aqueous systems can be achieved with self forming gradient solutions of salts [29]. A perfect salt gradient would have a high molecular weight and a large diffusion coefficient for rapid gradient formation, as well as a low viscosity so that lipoprotein migration to isopycnic density ranges is not impaired [31]. These properties can be achieved by coalescing a heavy metal cation to a highly soluble organic ligand anion to produce a compact, but high molecular weight solute.

Currently, an appealing ligand to use consists of the ethylenediaminetetraacetic acid (EDTA) as it offers the ability to have an ever changing molecular weight due to the interchangeability of its ions and counterions. Our laboratory currently employs EDTA complexes of Cu, Fe, Cd, Pb, and Bi using Na^+ and Cs^+ counterions. Depending on the separation of lipoproteins desired, any one of these novel self generating density

gradients can be chosen. Figure 5 depicts two of these gradients ultracentrifuged with the same serum sample of a patient in relatively decent health, meaning that no signs of an atherosclerotic condition.

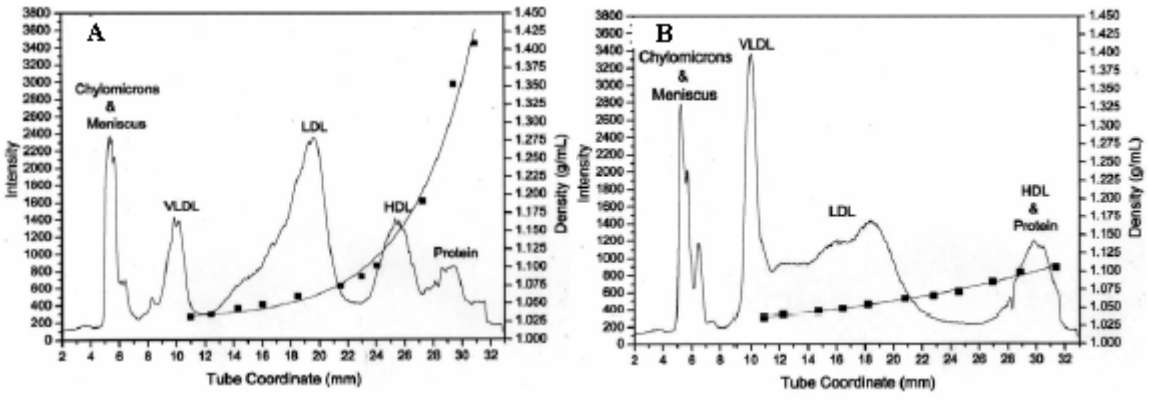

Fig. 5. Density serum lipoprotein isopycnic separation using CsBiEDTA gradient (A) and $Na_2CdEDTA$ gradient (B). LDL features are enhanced in profile B [32].

EDTA complexes containing bismuth achieve a near baseline separation among the five major separation bands of human serum. The major separation bands are Chylomicrons, VLDL, LDL, HDL, and protein. A gradient of this sort is typically used for initial screening of patient's serum as it offers a complete profile of all lipoprotein classes. Unfortunately, a full profile can mask great detail in any one of the lipoprotein classes. The image on the left in figure five depicts a stepped LDL band, meaning that possible subclasses of LDL are present. The image on the right in figure five utilizes a Na2CdEDTA gradient which has a nearly linear density slope making its gradient much less steep than others. This type of gradient allows the LDL class of lipoproteins to be widened to a great degree allowing subclasses to be examined if the patient possesses

them. The importance of LDL subclasses has been previously discussed, and due to the great broadening of the LDL band by the $Na_2CdEDTA$ gradient, it is possible that analysis of the subclasses can be accomplished through simple imaging techniques. For these reasons, the sodium-cadmium based gradient has been chosen for the research presented in this thesis.

Imaging/Analysis of Lipoproteins

Once lipoprotein banding is achieved via an ultracentrifuge and chosen density gradient, the lipoproteins can then be subjected to image analysis depending on the way the lipoproteins were prepared. Typically, lipoproteins are stained or dyed to enhance their visibility in ultracentrifuge tubes allowing imaging of the bands to be much easier. Common imaging probes used are protein stains, lipophilic stains, or fluorescent phospholipid probes.

Protein stains such as Coomassie Brilliant Blue R (CBBR) typically associate themselves with lipoproteins through an ion-pairing interaction [27]. A different number of dye molecules are bound to each of the apolipoproteins on the surface of lipoproteins and the values are dependent on the basic amino acid content [33]. Since dyes of this nature are dependent upon protein conformation, it is safe to assume that the number of dye molecules associated with each lipoprotein is heavily influence by the lipoprotein's protein content, size, and protein conformations. The unpredictability of lipoproteins as well as the patient to patient variability makes quantitative lipoprotein determinations using protein stains nearly impossible.

Lipophilic stains like Fat Red, Sudan Black B (SBB), and nitroblue tetrazolium (NBT) have been used to relative success, but these techniques fail to present quantitative

results as well [34,35,36]. The majority of lipophilic dyes take numerous hours to penetrate the lipoproteins through partition diffusion and many see no saturation of the lipoprotein particle within a reasonable time frame [37]. Stains of this nature have also shown dependencies on certain types of lipids found in lipoproteins making quantitative analysis nonexistent.

Fluorescent phospholipid analogs have been proven to be extremely useful in lipoprotein analysis as they are effective at low concentrations not affecting the natural characteristics of the lipoprotein. They also incorporate themselves on the surface of the particle much like the native phospholipids do [38]. One of the widely used molecular probes of this nature is N-[7-(4-nitorbenz-2-oxa-1, 3-diazole)]-6-aminocaproyl sphingosine (C_6-NBD-ceramide) and figure 6 depicts its structure.

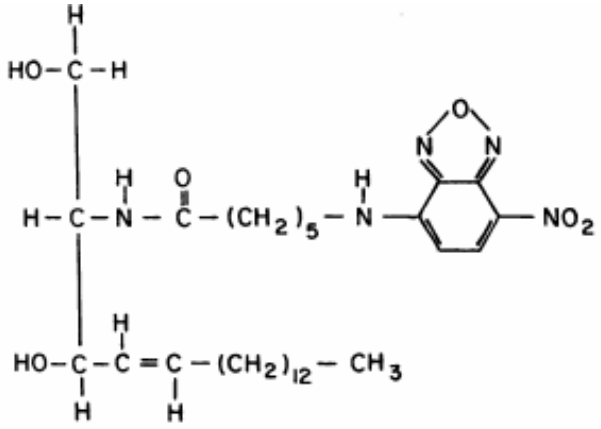

Fig. 6. Structure of C_6-NBD-ceramide [39].

The C_6-NBD-ceramide molecule imbeds itself into the membrane layer of the phospholipid with the polar region at the surface and the fatty acyl chain extending deep

into the non-polar membrane region. Interestingly, the other smaller fatty acyl chain that has the NBD fluophore bound at its end, curves to the polar surface of the membrane due to the hydrophilicity of the NBD [40]. Since the majority of this fluorophore tagged molecule resides near the surface of the membrane, the time required for lipoprotein staining is highly decreased. In addition to this characteristic, NBD labeled lipids have a prime excitation wavelength of 466 nm with sharp emission spectra at 536 nm and resist fluorescence quenching to a high degree [40].

NBD ceramide can even be closely associated with true quantitative analysis since its uptake and amount of fluorescence has been loosely correlated to lipoprotein cholesterol concentrations. However, there are many drawbacks to this fluorescent probe prohibiting quantitative results. For example, in order to get quantitative concentration results, the serum sample must be introduced to a saturating amount of NBD so that full uptake of the fluorescent probe can be achieved. By doing this, two possible negative outcomes may result. One being that the amount of NBD needed for saturation may delipidate the lipoprotein particles since NBD ceramide is typically diluted in the organic solvent dimethyl sulfoxide (DMSO). Secondly, the increased uptake of the NBD fluorophore has been proven to affect the physical and chemical properties of the serum lipoproteins as the electrophoretic mobilities of the lipoproteins are slightly altered [41]. It is also believed that serum characteristics vary from patient to patient too greatly to generalize fluorophore uptake to specific lipoprotein classes for individual patients. In light of these disadvantages, NBD ceramide still serves as an outstanding qualitative tool, but innovations in the field are necessary.

Ideally, the best means of quantitation would be to use a component that naturally fluoresces within the lipoproteins, such as tryptophan. Making use of the lipoprotein's native light scattering characteristics would be an interesting method of quantitation as well. After lipoproteins are banded from ultracentrifugation, a molecule such as tryptophan contained within the lipoproteins could be excited allowing fluorescence of the lipoprotein molecules. This would eliminate the possible errors created by the numerous probes and there would be no more nuisances of long sample preparations. Although this is a very realistic approach, tryptophan has an excitation of 280nm and an emission of 355 nm [42]. Extremely powerful light beams in the ultraviolet range can be expensive and most UC tubes are made out of polycarbonate which absorbs in the UV range.

The best probable setup for lipoprotein quantitative analysis would most likely rely on simple light scattering as the foundation. Applying Mie and Rayleigh scattering theories to that of the banded lipoprotein particles, is promising. Variations of the Mie and Rayleigh light scattering theories make it possible to detect particle size, concentration, and even molecular weight. Utilizing light scattering techniques directly upon banded UC tubes has yet to be done and would be an innovation in the field allowing researchers to gain an unbelievable amount of data from a single UC spin. Experimental costs could be greatly reduced when molecular probes are subtracted from the equation.

Light Scattering

Light scattering is an omnipresent naturally occurring phenomenon that has captivated the great minds of science for centuries. In the late 15th century, Leonardo da Vinci (**ca. 1500**) provided a much generalized theory on the scattering of light:

> I say that the blueness we see in the atmosphere is not intrinsic color, but it is caused by warm vapor evaporated in minute and insensible atoms on which the solar rays fall, rendering them luminous. . . . Hence it follows, as I say, that the atmosphere assumes this azure hue by reason of the particles of moisture which catch the rays of the sun [43].

Leonardo da Vinci's insight about light's interaction has bounded forward to explain numerous natural effects and calculate a variety of data based on its interactions with matter. The properties of light can be easily harnessed or manipulated for multiple data acquisition experiments including particle size, molecular weight determinations, and particle concentration determinations.

Generally speaking, matter is composed of protons and electrons and they can be set into an oscillatory motion (an excited state) by incident electromagnetic radiation. These "excited" entities will either radiate a portion of the electromagnetic energy as they relax to their original state, or they will transform the electromagnetic energy into thermal energy or absorption, for example. This basic principle serves as the backbone for all electromagnetic wave scattering theories.

In the scope of this thesis, elastic scattering will be focused upon with additional attention being paid to the general theory of Rayleigh scattering and the specifics of Dynamic Light Scattering. Although all electromagnetic waves undergo some form of scattering or energy transformation, elastic scattering pertains to the radiation scattered at a frequency and wavelength equal to that of the incident radiation. The most popular

forms of elastic scattering used in science are Rayleigh light scattering and Mie light scattering. In contrast to elastic scattering, inelastic scattering is the process in which the incident electromagnetic energy is lost or gained resulting in changed frequencies and wavelengths of the scattered light. Some common applications of inelastic scattering would be Brillouin, Compton, and Raman scattering.

Rayleigh Scattering

The general premise of Rayleigh scattering is that because the particle is small compared to the wavelength of incident electromagnetic radiation, typically $d < (\lambda/10)$, that the instantaneous field which it experiences due to the electromagnetic wave is uniform throughout [44]. Even though the intense Lorenz-Mie theory matrices can be applied to Rayleigh type interactions, the complex mathematics do not adequately explain the light interaction with such a small particle. The Rayleigh scattering approximation was created on the same principles as the Mie scattering theory with the addition of particular parameters that allow easier calculations the characteristics of these nanometer sized particles.

When utilizing this theory on its most basic of levels, a researcher must be aware of the critical boundaries of the equation. For example, when applying the Rayleigh equations, it is assumed that the aqueous suspension medium is homogeneous, the scattering from the particle is isotropic, the particles have a diameter of less than the wavelength divided by 10, and most importantly that single independent scattering exists. The last boundary condition implies that multiple scattering off of one particle is minimal and that each particle is exposed to the incident radiation. If all boundary conditions are

met, and assuming unpolarized incident radiation, than one can utilize the following Rayleigh scattering equation [45]:

$$I = I_o (\pi^4 d^6 / 8\lambda_o^4 R^2) * [m^2\text{-}1 / m^2\text{+}2]^2 * (1+\cos^2\theta) \quad (3)$$

where I is the scattered light intensity, I_o is the incident light intensity, d is the diameter of the particle, λ_o is the vacuum wavelength of the incident radiation, R is the distance the scattered light has to travel to detection, and θ is the angle of scattered radiation with respect to the plane of incident radiation. Finally, m is the complex refractive index ratio given by:

$$m = (n_2\text{-}ik_2) / (n_1\text{-}ik_1) \quad (4)$$

where the subscript of 2 indicates the sphere and the subscript of 1 indicates the surrounding medium. The refractive index is indicated by n, and k is the extinction coefficient. Initially, the "basic" Rayleigh scattering equation appears very intimidating, but when the conditions of our laboratory's camera system #2 (to be explained later) are applied to this equation, many factors can be reduced significantly.

The Rayleigh scattering Intensity equation listed above is actually the equation for Rayleigh scattering produced by unpolarized light. This formula combines two separate forms of the equation in regards to perfectly linearly polarized light as well as perfectly perpendicularly polarized light. This is applicable if the scattering sphere is sufficiently small and the scattering detector is positioned perpendicular to the path of incident radiation. When illuminated by unpolarized light, then the scattered light is 100%

polarized at a scattering angle of exactly 90^{o} from the plane of incidence. The angular distribution of Rayleigh scattering essentially sums up this concept of polarization and is depicted in figure 7 [46].

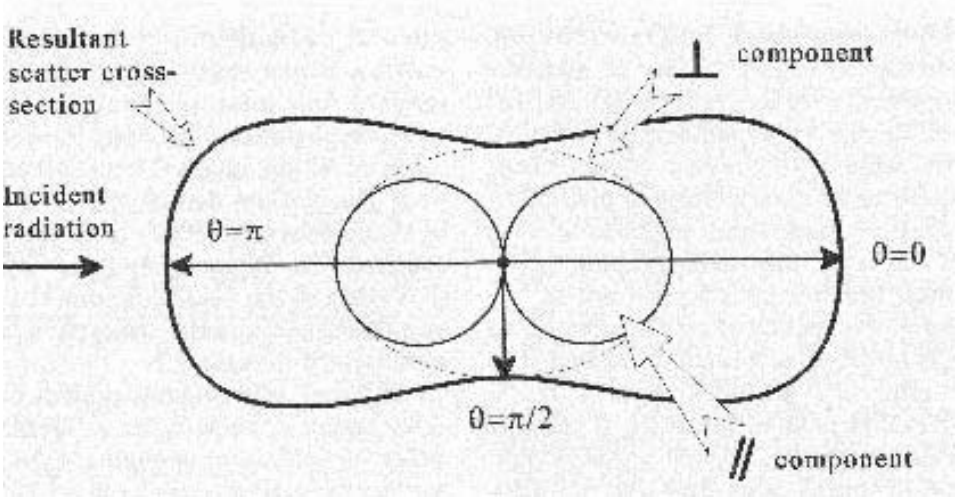

Fig. 7. Schematic of the angular distribution of Rayleigh scattering [46].

In addition to this, if the refractive index of the medium is within a reasonable proximity to that of the scattering particle and the spheres are considered transparent, meaning that they are small enough that they will either scatter the light or the light will pass right through. The complex refractive index ratio can now be reduced to (n^2-1 / n^2+2), where n now simply refers to the refractive index of the particle [47]. In the end we are left with:

$$I = I_o (\pi^4 d^6 / 8\lambda_o^4 R^2) * (n^2\text{-}1 / n^2\text{+}2)^2 \quad (5)$$

This particular equation relates to the scattered intensity of one spherical particle with a diameter of no more than one tenth of the wavelength of incident radiation. Since most samples analyzed will have more than one particle scattering light, it would be necessary to develop an equation that could be more relative to a typical sample of particles of low concentration. Low concentration is stressed as high concentration systems would undoubtedly allow multiple scattering and high inter-particle interactions.

The angular distribution of Rayleigh scattering is governed by the scattering angle. At an angle perfectly perpendicular to the incident radiation, the light scattered forwards and backwards will be of identical intensities. In addition to this, my research design takes into account a sphere in a surrounding medium such as water with an associated refractive index of n_{med}, and this causes the vacuum wavelength of light, λ_o, to be replaced by the wavelength of the light in the medium, λ_o/n_{med} [48]. The total scattering cross section can now be obtained by integrating the Rayleigh equation over the area of the sphere representing the (σ_s) [48]:

$$\sigma_s = (2\pi^5 d^6 n_{med}^4 / 3\lambda^4) * (n^2\text{-}1 / n^2\text{+}2)^2 \qquad (6)$$

It should be noted that prior to integration, the irradiance was multiplied by the area subtended by the solid scattering angle and this yielded the total power scattered into the angle of irradiance. This is how the previous term for path length, R, disappears through the integration step. The scattering cross section presented here appears to neglect the actual number of scattering particles present, but this value is taken into account when the light intensity is related to the scattering cross section.

At this point, it is now necessary to reinforce the relationship between light intensity and the scattering cross section so that diameters of particles can be distinguished. Essentially, the classic Beer-Lambert law can be manipulated to fit our needs and it becomes the integral equation tying light intensity to the scattering cross section term which in turn relates to the particle diameter. If the particle concentration or particle density, ρ, is considered to be sufficiently low, then it can be assumed that the light will most likely be scattered only once when traversing the solution. Bound by the single scattering condition and the fact that absorption can be neglected due to size, the scattered irradiance I_s after traveling through the medium a distance of *R,* can be related to the incident irradiance I_o [48].

$$I_s = I_o e^{-\rho\sigma R} \tag{7}$$

This equation can then be transformed to the scattering cross section [48].

$$\sigma_s = -\left(\ln(I_s/I_o) / \rho R \right) \tag{8}$$

However, the intensity seen by the detector/camera is known as the optical density, D, since the intensity being scattered from the sample is dependant upon the density of the sample.

$$D = \log (I_o / I_s) \tag{9}$$

The optical density equation can be solved for the experimental cross section, but since the particle is so small, absorption can be ignored and the experimental cross section becomes the scattering cross section, σ_s.

$$\sigma_s = (D*\ln(10)) / (\rho R) \quad (10)$$

Utilizing this equation, light intensity is now related to the scattering cross section and when this value is calculated, the scattering cross section can be used to back calculate the particle diameter mentioned earlier in this mathematical derivation. Unfortunately, these mathematical equations can not be properly applied to our laboratory's research at this time.

In order to experimentally calculate scattering cross section, one must be knowledgeable of the particle concentration scattering the light. At this point, the concentration unknown is difficult to establish within our laboratory as the samples being imaged are based upon equilibrium density separations achieved through an ultracentrifuge. To properly calculate this equation, the particle concentrations would need to be known at every point through out the vertical length of the ultracentrifuge tube. This has yet to be determined making it difficult to calculate the scattering cross section and determine the individual particle diameters banded throughout the tube. Although this aspect is somewhat discouraging, it has been postulated that using an internal standard of a known size and concentration, a calibration curve could be established allowing proper estimation of concentrations throughout the banded

lipoproteins. A proper surrogate particle has yet to be properly harnessed allowing us to complete a calibration curve this sort.

Quantitatively, the Rayleigh approximation is widely used regularly on systems that that strictly obey the aforementioned parameters. Although this approximation can be applied to my research, there are still a few experimental achievements awaiting completion so that this series of equations can be properly applied. At this point, the Rayleigh theory serves extremely well as a qualitative technique. The strong wavelength dependence (λ^{-4}) of the theory dictates that a light in the boundaries of blue light scattering intensity would be the most intense. More importantly, it should also be noted that the diameter of the particle has an enormous bearing on the resulting scattered intensity and the amount of scattering particles present has a reasonable implication on the resulting intensity. The diameter of the particle has a much larger influence on the light scattered than the particle concentration. With knowledge of the importance of the effects of diameter and particle concentration, very important qualitative data can be expressed. In addition to current qualitative data recorded about the density separated lipoproteins, an immense amount of detail about the patient's health can be diagnosed.

Dynamic Light Scattering

Dynamic Light Scattering, synonymous with Photon Correlation Spectroscopy (PCS) and Quasi-Elastic Light Scattering (QLS), is a very sensitive and well established technique that allows accurate particle size determinations of substances suspended in solution. In general, the correlation of scattered light intensity is measured as a function of time. In this technique, the random movement of particles due to various random

collisions between the suspended particles and the known molecules in the dispersing fluid serves as the foundation of the measurement. This foundation is better known as Brownian motion.

Brownian Motion. The term Brownian motion (in honor of the botanist Robert Brown and his experiments regarding pollen) refers to the physical phenomenon that minute particles, immersed in a fluid, move about randomly [49]. Using this concept, it can be assumed that larger particles will move slower than smaller particles as they would need much more randomly external forces to be placed in motion. The velocity of the Brownian motion can be defined by the property widely known as the translational diffusion coefficient (D) and the size of the particle is calculated from the translational diffusion coefficient by using a version of the Stokes-Einstein equation [50].

$$d(H)= (kT)/(3\pi\eta D) \tag{11}$$

where d(H) is the hydrodynamic diameter, k is the Boltzman's constant, T is the absolute temperature, η is the coefficient of viscosity, and D is the translational diffusion coefficient.

The hydrodynamic diameter is the diameter obtained by this technique as it directly relates to the diameter of a standard sphere that has the same translational diffusion coefficient as the observed particle. Since all particle sizing instruments rely on the particle being suspended in a medium, this equation is chosen for proper computation.

The original Stokes-Einstein relationship describes the Diffusion coefficient only in regards to the particle's radius which is represented by the symbol r.

$$D= (kT)/(6\pi\eta r) \quad (12)$$

In addition to this, the original Stokes-Einstein relationship states that the diffusion coefficient relies on the viscosity as well. Although the equation for the coefficient of viscosity, η, is essentially straight forward, there are a few hidden chemical and physical properties that will influence the mathematics. Shape, surface structure, and ionic strength of the medium are influential parameters and they will be explained later in this section. The coefficient of viscosity is defined as;

$$\eta = Fl/\nu A \quad (13)$$

where η is the coefficient of viscosity, F is the Force, A is the area, ν =is the speed, and l is the separation length [51].

Doppler Shift. The main principle behind dynamic light experiments has been explained, but a large portion of the technique has yet to be explicated. Even though the basis of Brownian motion has been spoken about, there is still a hole in the theory connecting the use of incident radiation, scattered radiation, and the diffusion coefficient. The Doppler Effect, named after Christian Andreas Doppler, fills in the final puzzle pieces of how data is actually gathered from a general point of view.

In regards to Doppler shift, a ray of incident radiation of a known frequency is directed upon the desired particle undergoing Brownian motion and the scattered light from the particle will most likely be at a slightly different frequency. This difference in frequency can be considered a shift in frequency. Smaller moving particles will create a much larger shift in scattered frequency and larger particles will show a smaller shift in frequency. The frequency shifts observed using incident radiation is identical to the change in sounds heard by the siren of an ambulance passing a stationary observer. The frequency shifts observed over time will be used to determine the relative velocity of the particles undergoing Brownian motion, and this data will then be related to hydrodynamic particle size distributions.

To calculate the speed of the velocity of the particle under Brownian motion using the Doppler shift, one would utilize one of the two following equations. For the velocity of the particle moving toward the observer (light probe), you would use;

$$f' = [1/(1-(\upsilon_s/\upsilon)]*f \tag{14}$$

where f' is the new frequency, f is the original frequency, υ_s is the speed of particle, and υ is the speed of light.[51] For the velocity of the particle moving away from the observer (light probe), you would use;

$$f' = [1/(1+(\upsilon_s/\upsilon)]*f \tag{15}$$

where f' is the new frequency, f is the original frequency, υ_s =is the speed of particle, and υ is the speed of light [51].

Accuracy of DLS Diameter Measurement

From intensely reviewing the factors affecting the diffusion coefficient as well as the Stokes-Einstein equation, it quickly becomes evident that there are numerous intricacies that can adversely affect the accuracy of the diameter measurement. In regards to the Stokes-Einstein equation, a large constraint put on the accuracy of the data lies within the temperature (T). The hydrodynamic diameter obtained of DLS experiments is directly proportional to and relies heavily on the accuracy on the temperature. The temperature can drastically affect the viscosity of the sample resulting in distorted diffusion speeds of the particles. Malvern Instruments report that for an aqueous dispersion measured at a temperature close to 25^{o}C, every 1^{o} error in the temperature will result in a 2% error in the size obtained [52]. Fortunately, the Microtrac Nanotrac DLS instrument used in the research presented is designed for room temperature analysis making drastic temperature fluctuations a rarity.

Factors Affecting Light Scattering

Ionic Strength of Medium. One must take into consideration the ionic strength of the particle's medium as the ionic strength may directly affect the electric double layer of the analyzed particle. In our case, univalent and divalent EDTA salts are used as a density gradient and particle sizing medium. The ionic strength of the medium will have a bearing on the thickness of the electric double layer of the particle, better known as the Debye-Hückel length (k^{-1}), and this thickness will affect the diffusion speed of the particle. The electric double layer pertains to the development of a net charge at the

particle's surface causing an increased concentration of counter ions from the medium to build up at the surface of the particle (see figure 8) [53].

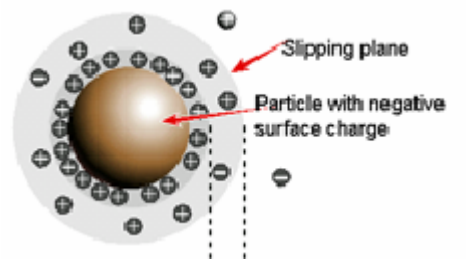

Fig. 8. Representation of a particle's electric double layer (Debeye Length) [53].

In a dilute suspension, the overall thickness of the electric double layer is related to the ionic strength *I* of the suspension by [54,55].

$$k^{-1}(\text{nm}) = (2000e^2 N_A I / \epsilon K_B T)^{-1/2} \quad (16)$$

where, e is the elementary charge, N_A is Avagadro's Number, ϵ is the dielectric constant of medium, K_B is the Boltzman Constant, and T is the absolute temperature. The ionic strength of the solution can be calculated using the following equation.

$$\text{Ionic strength} = \mu = \tfrac{1}{2}([A]Z_A^2 + [B]Z_B^2 + [C]Z_C^2 + ...) \quad (17)$$

Where [A], [B], [C], . . . represent the molar species concentrations of ions A, B, C, . . . and Z_A, Z_B, Z_C, . . . are their respective ionic charges [56]. If the electrolyte of molar

concentration C is symmetrical (Z-Z charge) at room temperature, then equation 16 can be reduced to a much simpler form.

$$k^{-1}(\text{nm}) = (3.29Z\sqrt{C})^{-1} \quad (18)\ [55].$$

Essentially, it can be said that a high ionic strength (high solution conductivity) will result in suppression of the electrical double layer of the particle as well as the measured hydrodynamic diameter. Reniliang Xu published an article stating that the most accurate dynamic light scattering particle size determinations need to be made under high ionic strength mediums with conductivity greater than 1 mS/cm [55]. In addition to this information, it has also been mentioned that under extremely high ionic strengths that the double-layer thickness can decrease to such a degree that interparticle forces, such as Van Der Wall's forces, will clearly dominate allowing very densely populated flocs to form [57]. Too small a medium conductance can produce a lengthened electric double layer leading to a reduction in diffusion speed and a larger determined diameter. Although somewhat convoluted, it appears that there is an acceptable zone of Ionic strength for DLS measurements and our laboratory's novel density gradients appear to be well within the established criteria.

Surface Structure of Particle. Another example of a particle parameter that can adversely affect the diffusion coefficient is the surface structure of the particle being analyzed. The surface structure of the particle can falsify particle size determinations in

regards to both Rayleigh scattering approximations as well as Dynamic Light Scattering experiments.

Considering DLS, a consistent spherical shape will cause a consistent diffusion speed as well as consistent scattering for the particle. However, if the particle's surface contains portions of "roughness", then the calculated diameter could vary by a few nanometers as the diffusion speed of the particle will be altered as the particle inconsistently travels through the medium. Although unlikely, highly ionic mediums can dictate conformational changes of proteins present on the surface of a lipoprotein causing extreme surface "roughness" and altered diffusion speeds. The low ionic and low molarity of the EDTA gradients used in our analysis makes these changes unlikely.

In regards to Rayleigh scattering techniques, random discrepancies in the surface structure/roughness of the naturally occurring low density lipoprotein particles have an insignificant bearing on particle size determinations. The degree of surface roughness is typically defined by the parameter η that incorporates the roughness displayed by the particle over the wavelength of incident radiation [58]. For extremely small particles like low density lipoproteins, this parameter would have to be fairly significant for the determined diameter to be affected. If this ratio was ever capable of getting to such an elevated state, the particle will most likely no longer be considered spherical causing the Rayleigh approximation to no longer be appropriate. Since the lipoprotein diameter is so small compared to the wavelength of incident radiation, I have disregarded all possible effects due to surface roughness.

Particle Shape. Another illustration of a particle's characteristics affecting the diffusion coefficient and other light scattering data is the particle's shape and orientation. For example, a cylinder's length has a much larger bearing on its effective diffusion speed when compared to slight changes in the cylinder's diameter. The diffusion speed will be altered more by the length of the cylinder as that will cause more drag as the particle moves throughout the medium. A cylinder with a slightly larger radius but a slightly shorter length will have a faster diffusion speed through the medium. Although the two cylinders are close in overall size, the cylindrical particle with a longer length will be determined to have a much larger diameter.

On the other hand, Rayleigh scattering size measurements are not affected by a differing diffusion speed like DLS experiments are. However, Rayleigh experiments can be greatly affected by the particle's shape as well as its orientation. Irregular shaped particles will give a shift in the median size and a more pronounced broadening of the apparent size distribution [59]. The broadening of the distribution can be the direct result of the irregular shape or the orientation of the particle. For instance, imagine an exaggerated ellipsoid with the incident radiation incoming from the left side on the x-plane. Depending on the orientation of the particle, a large diameter or a small diameter may be recorded (see figure 9).

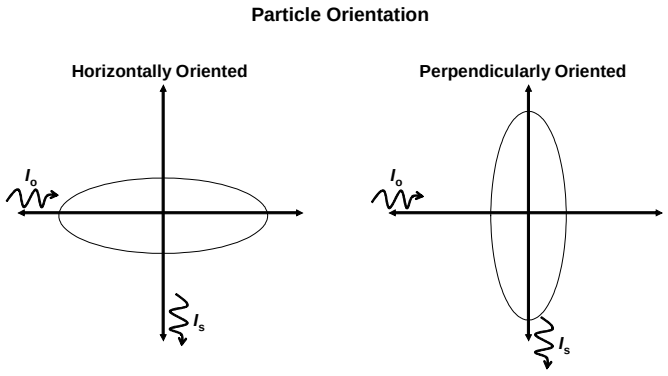

Fig. 9. Effects of lipoprotein particle orientation.

Utilizing our laboratory's 90 degree angle of scattering, one can see how the orientation of the scattering article would alter the intensity of the scattered radiation. The ellipsoid would result in false size data in both orientations as well as violating the Rayleigh strict boundary conditions. To accurately calculate the non-spherical particle's diameter, one would have to use an extension of the Mie theory that covers the full conditions of the analysis. A laundry list of Mie theory extensions can be found in Thomas Wredt's paper, "A Review of Elastic Light Scattering Theories" [60].

Thankfully, the lipoproteins are assumed to be spherical and this characteristic has been determined through TEM experiments on low density lipoprotein molecules. Figure 10 depicts TEM images of lipoprotein particle Lp(a).

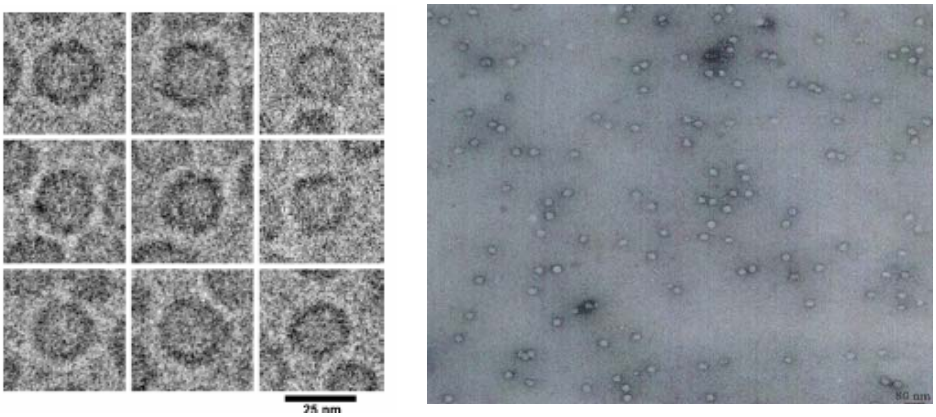

Fig. 10. TEM images of lipoprotein(a) [25,61].

The image on the left in figure 10 is a tunneling electron micrograph (TEM) of Lp(a) particles obtained by Rik van Antwerpen and the image on the right of figure ten is of the same particle, but is was obtained by the research of Leticia Espinoza [25,61]. The TEM images show the particles to be in the 25-35 nm range in diameter and both show the particles to be very spherical. Since Lp(a) is a subclass of low density lipoproteins, it can be assumed that the rest of the low density lipoprotein class would have spherical characteristics as well. Because of this, the Rayleigh approximation is valid and the shape of the particle is a negligible characteristic in the size determination.

DLS Particle Size Analysis Innovations

The basic DLS techniques apply to all common particle sizing instruments, but innovations still arise throughout the field. The Microtrac Company sets themselves apart from the rest of the industry as they use a heterodyne configuration for their

dynamic light scattering instruments as opposed to a homodyne configuration. The following figure, figure 11, better explains the difference between the two configurations employed to obtain Brownian motion data based upon Lorentzian functions of frequency shifts of the light.

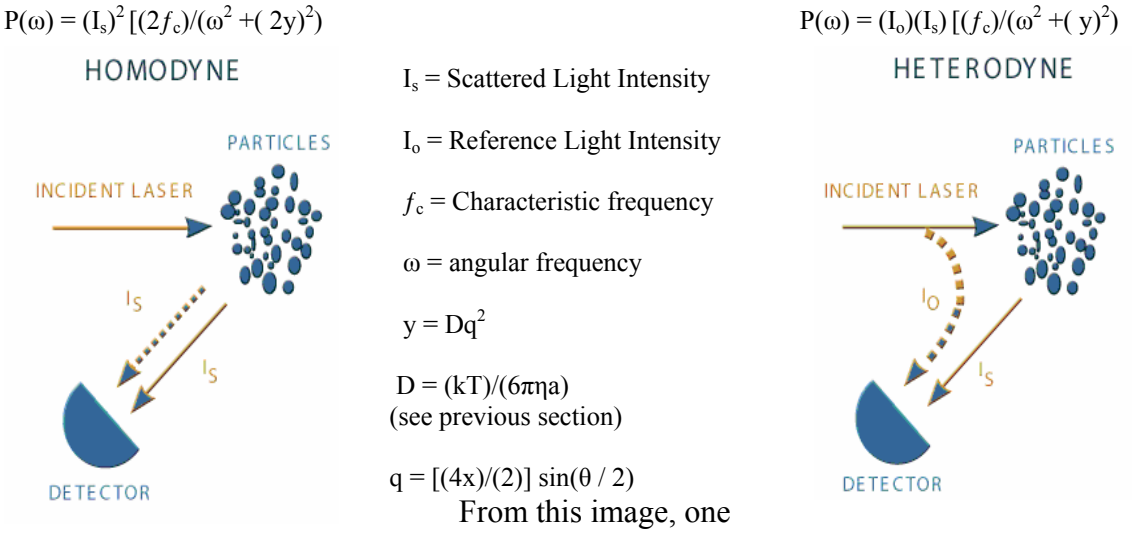

Fig. 11. Homodyne and heterodyne scattering configurations [62].

The benefits of the heterodyne configuration are clearly visible in figure 11. The non-shifted light performs as a stable reference point for the instrument to compare the shifted and scattered light to. Although other instruments utilizing the homodyne configuration incorporate a baseline reading as well, these instruments utilize a reference based upon light traveling through the mobile media at an angle where scattering of the important sizing frequencies is minimal. The immense difference between the two configurations lies solely within the inherent detection capabilities of the two.

Under the homodyne configuration, the power spectra is proportional to the scattered light Intensity squared, (I^2), while the heterodyne power is proportional to the scattered intensity multiplied by the reference intensity. By examining this difference, one can see how the heterodyne configuration can be capable of having much higher power spectra. Depending on the reference frequency, this intensity signal can be quite large when compared to its homodyne counterpart. Generally speaking, this increased power concept allows for the measurement of very small particles at low concentrations resulting in heightened sensitivity.

With the Heterodyne configuration being an integral part to the success of the instrument's determinations, Microtrac did not stop at one design breakthrough. The following figure illustrates the instrument's patented probe design.

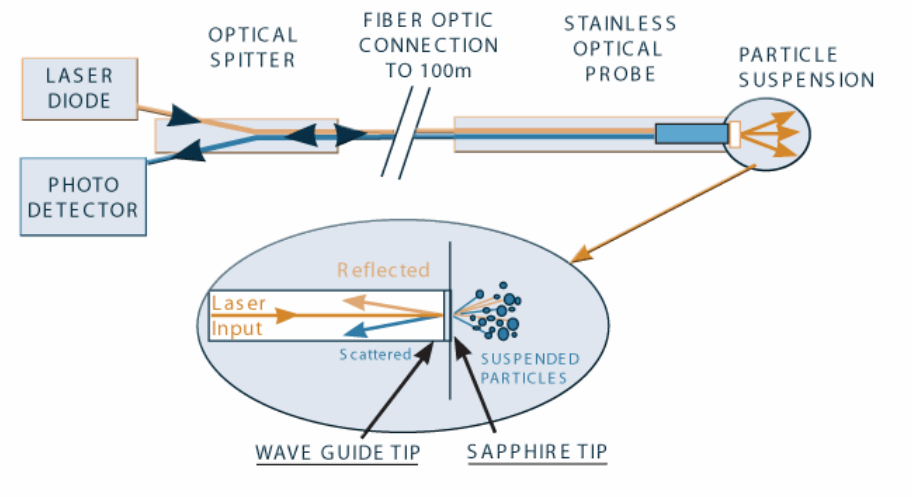

Fig. 12. Microtrac's Nanotrac 250 instrument overview [62].

The Microtrac Nanotrac 250 utilizes a fiber optic waveguide fitted with a sapphire window at the tip making the instrument very versatile. The sapphire window embodies a very high refractive index allowing a portion of the incident radiation to be reflected and used as the reference beam.

Overall, light from the infrared laser diode (3 mW, Class IIIB) is emitted at a wavelength of 780 nm and it travels down one arm of the waveguide to the sapphire window. The second arm of the probe allows the light that passes through the sapphire window to enter the solution. The third arm of the probe allows the backscattered light and the reflected reference light to travel towards the photo detector. Since the probe incorporates a window that internally reflects the reference beam, the instrument can utilize a very short path length of backscattered light (scattered at 180^{o}) from the analyzed particles. The short path length indicates that the incident radiation that does immediately backscatter will simply pass through, scatter at a different angle, or will be lost through multiple scattering interactions. Since only the particles closest to the tip of the probe have the best chance for backscattering, this measurement technique can be applied to solutions of high concentrations. The scattered light analyzed does not penetrate extremely far into the sample preventing adverse optical effects as well as multi scattering, resulting in accurate particle size determinations.

The intensities of the reference and scattered beams enter the detection portion instrument where a common silicon photo detector as well as a solid-state laser diode source is housed. It is mentioned that this combination of detection is very stable and reliable. The power spectrum outputted by the detector setup is then calculated with a high speed Fast Fourier Transform digital signal processor. The finalized power

spectrum is then further calculated in the proprietary software that relates the velocity of the particles under Brownian motion and the diffusion speeds of the particles to a particle size distribution. Although the specificity of the calculations is not fully disclosed, it can be assumed that the calculations would be very similar to other scattering instruments that utilize a correlation function.

The correlation function essentially correlates the random Brownian motion with the fluctuations of scattered intensities as a function of time [50].

$$G_{(\tau)} = \langle I(t).I(t+\tau) \rangle \tag{19}$$

Where τ is the sample time of the correlator and I is the intensity measured. Since the samples being analyzed are polydispersed after excision and thawing, a specific version of the correlation function is most likely used that incorporates the sum of all the exponential decays contained in the correlation function.

$$G_{(\tau)} = A[\ 1 + B\ \Sigma(\exp(-2\Gamma\tau))] \tag{20}$$

Where A is the baseline of the correlation function, B is the intercept of the correlation function.

$$\Gamma\ = Dq^2 \tag{21}$$

$$Q = (4\pi n / \lambda_o) \sin(\theta/2) \tag{22}$$

Where n is the refractive index of dispersant, λ_o is the wavelength of incident radiation, θ is the scattering angle [50]. Once the correlation function is determined, the size is obtained from fitting a multiple exponential to the function to obtain the distribution of particle sizes.

EXPERIMENTAL

Chemicals

$Bi_2O_2CO_3$, H_4EDTA, Cs_2CO_3, $CdCO_3$, Na_2CO_3, agarose coupled wheat germ agglutinin (L-1882), phosphate buffered saline (PBS) tablets, phosphorylase *b*, and N-acetyl-D-glucosamine were obtained from Sigma Aldrich (St. Louis, MO). Sucrose was purchased from EMD Chemicals Incorporated (Gibbstown, NJ). The Apo B-100 turbidimetric immunoassay kit (993-27401) and the apolipoprotein calibrator (992-27591) were obtained from Wako Chemicals (Richmond, VA). The fluorescent probe NBD C_6-Ceramide was purchased from Molecular (Eugene, OR). Duke nanospheres (3020A, 3030A, 3040A, 3060A) were obtained from Duke Scientific (Freemont, CA). Invitrogen nanospheres (C37261, C37262) were purchased from Invitrogen (Carlsbad, CA).

EDTA Density Gradient Synthesis

The various EDTA salt complexes were synthesized from H_4EDTA in a procedure similar to that of Davidovich [63,64]. The reagents were then combined stoichiometrically in 100 mL of DI H_2O, followed by a 2-h reflux, yielding a clear solution. Depending on the desired complex and the starting materials, sodium carbonate of cesium carbonate was then added to the clear solution to bring the final pH range to 6.5-7.5. The final solution volume was reconstituted to 100 mL to account for evaporation during reflux to yield stoichiometric solutions with a final concentration of 0.200 M. At this point, these solutions can be diluted slightly to achieve a variety of density slopes depending on the application [32].

For CsBiEDTA:

$$2H_4EDTA + Bi_2O_2CO_3 + Cs_2CO_3 \rightarrow 2CsBiEDTA + 4H_2O + 2CO_2$$

For $Cs_2CdEDTA$**:**

$$H_4EDTA + CdCO_3 + Cs_2CO_3 \rightarrow Cs_2CdEDTA + 2H_2O + 2CO_2$$

For $Na_2CdEDTA$**:**

$$H_4EDTA + CdCO_3 + Na_2CO_3 \rightarrow Na_2CdEDTA + 2H_2O + 2CO_2$$

Measurement of EDTA Gradient Profile

Using any of the EDTA gradients, an ultracentrifugation spin was performed so that the equilibrium gradient forms identical to that of a sample containing serum. The gradients used within this thesis all reach equilibrium within six hours. A 1 mL aliquot of the chosen gradient is dispensed into a 1.5 mL, thick walled, polycarbonate ultracentrifuge tube (Bechman-Coulter). The tube was then placed into a 30^o fixed angle TLA 120.2 rotor and ultracentrifuged in a Beckman Optima TLX-120 ultracentrifuge for 6 h at 120,000 rpm and 5 ^{o}C. Upon completion of centrifugation, a 20-uL Pipetman pipet (P-20, Rainin Instruments, Woburn, MA) was fixed to a ring stand mounted on top of a stainless steel positioning lift (E36-283, Edmund Industrial Optics). This apparatus was used to accurately position the pipet tip in specific locations in the spun ultracentrifuge tube. The Microfire camera (S99808, Optronics, Goleta, CA) was used to image the vertical pixel location of the pipet tip upon retrieving a sample from the spun tube. Aliquots were removed from the tube in the range of 10-34mm. The vertical pixel values can be related to vertical tube dimensions as described by both Brain Hosken and Jeff Johnson [27, 32]. An aliquot was removed approximately every 2 mm in a descending

fashion until 10 aliquots were removed from each tube. The refractive indexes of the aliquots were then measured by a Bellingham & Stanley refractometer (60/DR, Lawrenceville, GA) at room temperature. The refractive index was then converted to density and graphed against the associated tube coordinate to achieve an accurate density curve for each EDTA gradient.

Blood Draw and Serum Collection

Blood from normolipidemic subjects was drawn into Vacutainer-brand series collection tubes following a 12-h fast via venipuncture at a Scott & White clinic. The 8mL tubes were treated with a silica clotting activator and packed with a minimal amount of separation gel (Beckton Dickinson Systems, Franklin Lakes NJ) prior to blood draw. Blood serum was then separated from the red blood cells by a 20 minute centrifuge spin at 3200 rpm and 4 ^{o}C. The supernatant was aspirated from the red blood cells and separated into 225 uL aliquots. The aliquotted serum samples were either immediately subjected to analysis or stored at -86 ^{o}C.

Separation of Lipoprotein Particles via Ultracentrifugation

EDTA Gradient Ultracentrifugation

1100 uL of the chosen density gradient (CsBiY, Na_2CdY, of Cs_2CdY) was dispensed into a 1.5 mL Eppendorf tube and 100 uL of serum was added to it. This solution was uniformly mixed by means of a vortex set at 1200 rpm. If the sample is chosen to be stained, then 10 uL of 1mg/mL NBD C_6-Ceramide diluted with DMSO is added. A staining span of 30 minutes is given so that the serum lipoproteins are capable

of complete uptake of the stain. After serum staining or after the initial mixing, a 1000 uL sample of the mixed sample is aliquotted from the eppendorf tube and is placed in the 1.5 mL ultracentrifuge tube. For all samples to be imaged by Rayleigh scattering, they are filtered through a Millipore 0.25 micron filter (SLGV004SL, Billerica, MA) in order to remove all dust particulates that will interfere in the scattering experiment. The tube is subjected to a 6-h ultracentrifuge spin at 120,000 rpm and 5 ^{o}C. After a spin, the samples are layered with 150 uL of DI H_2O so that the chylomicrons and VLDL classes are completely separated.

Sucrose Gradient Ultracentrifugation

Previously, 800 uL of a 20% sucrose solution was used as the rate separation medium and 400 uL of a diluted serum sample was carefully layered on top for ultracentrifugation. The diluted serum content consisted of 100 uL of serum added to 692 uL of DI H_2O [65]. However, this procedure does not allow comparative data with that of samples prepared in an EDTA gradient due to differing effective amounts of lipoproteins present in the ultracentrifuge tube. In addition to this, the final volume in a sucrose gradient tube equals 1200 uL while the final volume of an EDTA gradient equals 1000 uL. This difference in final volume does not allow direct comparisons either, since identical layering volumes can not be used affecting the separation between the chylomicron and the VLDL layers. For comparison sake, the sucrose gradient procedure was optimized.

By using 700 uL of a 16% solution of sucrose, 300 uL of a diluted serum sample can be carefully layered on top resulting in a final tube volume of 1000 uL. This final

volume allows sufficient room for identical layering techniques no matter the choice of gradient. Furthermore, the serum dilution step consists of 100 uL of serum being diluted with 260 uL of DI H_2O. Layering 300 uL of this dilution on top of the 700 uL of sucrose gradient allows a lipoprotein content equal to that of samples analyzed in EDTA gradients.

Lipoprotein Staining

The NBD C_6-Ceramide fluorophore is reconstituted to a density of 1 mg/mL by addition of dimethyl sulfoxide (DMSO) and is subsequently added to a sample. The serum sample is first added to the gradient and then the desired amount of NBD is added to the sample mixture. The fluorophore is given 30 minutes to fully stain the lipoproteins present.

Lipoprotein Imaging

All ultracentrifugation techniques are carefully layered with 150 uL of DI H_2O upon spin completion. Identical imaging techniques are performed with all gradients with minor differences only in the wavelength of incident radiation as well as the wavelength of emitted light. The recently developed imaging system incorporating an Optronics high resolution camera as well as a metal-halide light source with a collimated beam gives increased sensitivity and versatility to the lipoprotein image/analysis methods. The camera (S99808, Optronics, Goleta, CA) and Fiber-Lite metal halide light source (MH100A, Dolan-Jenner, Lawerence, MA) are placed orthogonally to each other

on an optical breadboard. Figure 13 accurately depicts the current geometrical configuration used for image analysis of the lipoprotein bands.

Fig. 13. Optical system for ultracentrifuge tube analysis.

A 2 mm slit is placed on the incident side of the tube holder so that excess light is prevented from interfering with the image through unwanted scattering effects. The wavelength filters used on both the excitation and emission side of the apparatus, in addition to shutter speed of the microscope camera can be widely adjusted depending on the experiment being conducted.

NBD Stained Serum Imaging

The NBD fluorophore is excited at 466 nm and emits radiation at 536 nm. These characteristics dictate the wavelength filters used to image the NBD stained lipoproteins. The filters (Schott, Elmsford, NY) used for proper analysis are a broad blue excitation filter (BG12) centered at 407 nm and a yellow cut-off filter (OG515) allowing wavelengths greater than 515 nm to pass through. It should be noted that filter BG12 has a sixty percent transmittance and a peak centered wavelength of 407 nm allowing a broad

range of wavelengths from 340 nm to 480 nm to pass through. Filter OG515 has a transmittance of ninety-one percent with all wavelengths greater than 510 nm. For comparative NBD images to that of Rayleigh scattering, a 2 mm optical slit is placed on the excitation side of the tube holder. A typical camera exposure setting used is 30 milliseconds.

Rayleigh Scattering Imaging

Rayleigh scattering image utilizes identical filters on both the excitation side as well as the emission side. For best results, the Rayleigh theory dictates that blue light of a small wavelength scatters the most amount of light. Because of this, a narrow band-pass filter of wavelength 455 nm was chosen. Unfortunately, this filter has a poor transmittance of fifty-two percent, but it does have an extremely narrow wavelength transmittance from 447 nm to 462 nm. This very narrow band prevents unwanted scattering, allowing only true Rayleigh scattering to be transmitted. A typical camera exposure setting used is 417 milliseconds.

Laser Rayleigh Scattering Imaging

A 5mw green laser pointer (GLE5sw-S, OnPoint Lasers, Minneapolis, MN) with a collimated beam of a wavelength equaling 532 nm is suspended on a ring stand vertically, ten inches above the ultracentrifuge tube. A VG9 emission filter is used on the camera and it has a transmittance of thirty-three percent with a centered peak wavelength at 521 nm and a transmittance range from 460 nm to 590 nm. A typical camera exposure used equals 240 milliseconds and this was used for the profiles presented in this thesis.

Image Analysis

The digital monochromatic images captured by the Microfire camera are transferred to a data file with a fire wire data transfer cable. The data file is stored on the associated computer for later use with the Origin software (Microcal Software Inc., Northampton, MA) supplied with the Microfire hardware. The Origin software converts the digital image to a data spreadsheet based on intensity per image pixel. A section that is 10 pixels wide located in the exact center of the tube and running the entire length is extracted and averaged for plotting purposes. The average intensities of the pixels are then plotted against their corresponding tube coordinates. For calibration purposes, all formulas are compared and adjusted to a standard UC tube with etched lines that have a known tube coordinate.

Lipoprotein Fraction Collection

It is necessary to excise the individual lipoprotein classes after ultracentrifugation if further analysis on the particles is desired. To accommodate this need, the ultracentrifuge tubes are slowly frozen in liquid nitrogen as to not disturb the gradient formation [66]. If frozen too quickly, the immediately formed ice crystals will randomly disrupt the precise density gradient. With a frozen sample, the lipoprotein fractions are sliced from the tube at predetermined and calculated positions with a high speed scroll saw (Model 1672, 16 inch, 2-speed, Dremel, Racine, WI) housing a thin 0.254 mm blade. The cut positions determined from the density profile are corrected for the expansion of the now frozen solid by equation 23 [27].

$$X_{frozen} = 1.0476 * X_{liquid} - 1.619 \quad (23)$$

Where X is the tube coordinate in millimeters.

Microtrac Particle Size Determination

UC tubes frozen by liquid nitrogen have the wanted lipoprotein fractions excised as previously discussed. The fractions are then thawed and centrifuged on a table top centrifuge at 3000 rpm for two minutes. The supernatant is aspirated and placed into a 1.5 mL eppendorf tube after passing through a 0.25 micron syringe filter. It is necessary to have the sample free from any debris as particle sizing is a very sensitive technique. It should also be noted that one must have at least 400 uL of sample for analysis, making duplicate fractions required when necessary. The fractions are dispensed into a cut and inverted bulb of a Samco transfer pipet (694 Q-PET, San Fernando, CA).

The probe of the Microtrac Nanotrac 250 (NPA250, North Largo, FL) can be lowered directly into the lipoprotein fraction. Once all bubbles are removed, the appropriate settings for measuring a human lipoprotein particle must be entered before analysis. In regards to this thesis, the parameters for a LDL like particle are displayed in table 3.

Table 3. Example of LDL particle sizing parameters using a Nanotrac 250.

Transparency	Transparent	**Fluid Refr. Index**	1.34
Particle Refr. Index	1.46	**Fluid Viscosity**	0.925
Particle shape	Spherical	**Fluid Temp. (C)**	23.49
Particle Density	1.04gm/cc	**Fluid Baseline**	DI H_2O

Depending on the lipoprotein fraction being analyzed, the particle density and the fluid refractive index may change. Both of these parameters can be determined form lipoprotein density profiling.

Determination of ApoB-100 Concentration

For this particular analysis, 3 uL of the same lipoprotein fractions subjected to particle sizing were placed in the center of a Beckton Dickinson microtiter plate (1172, Franklin Lakes, NJ) in triplicate along with the apoprotein calibrators. 175 uL of reagent buffer one was added to each sample, excluding the blank, and was immediately incubated at 37 ^{o}C for exactly 5 minutes. Using a Biotek Instruments µQuant ultraviolet/visible spectrometer, the absorbance of the samples was measured at a wavelength of 700 nm. This first reading corresponds to the sample baseline readings. 25 uL of reagent antibody two is then added to each well and incubated for another 5 minutes at 37 ^{o}C. At precisely 10 minutes, the final absorbance measurement is determined at 700 nm. The final absorbance is then calculated by subtracting the baseline absorbance from the second absorbance. The final ApoB-100 concentration is calculated

by the following equation.

$$\text{ApoB [ ]} = (\text{Abs. Of sample} / \text{Abs. Of Cal.}) * \text{Value of Cal.} \quad (24)$$

Lipoprotein(a) Differential Determination [25]

The concept behind this procedure is to analyze a serum sample for the presence of Lp(a) by means of lipoprotein density profiling. The Lp(a) is removed from a serum sample by complexing with wheat germ agglutinin through carbohydrate affinities. The Lp(a) depleted serum is then ultacentrifuged and profiled. The Lp(a) is recovered from the wheat germ agglutinin complex, mixed with density gradient, ultacentrifuged, and profiled like any other serum sample. The two density profiles are then compared to see if a noticeable amount of Lp(a) is present in the patient's serum.

Lp(a) Isolation From Serum by Lectin Affinity

Lp(a) is removed from serum by means of carbohydrate affinity of the apoprotein(a) through a sedimentation process. 50 uL of serum, 100 uL of PBS-200 mM praline (PBS-p), and 50 uL of agarose-WGA (0.336 mg of WGA/mL of gel packaged) are mixed together using a vortex mixer. The homogeneous mixture is incubated for 30 minutes at room temperature on a M-60 orbital plate shaker (Labnet International Inc., Edison, NJ). After incubation, a WGA-Lp(a) complex will be bound and can be sedimented out by slow table top centrifugation at a speed of 6000 rpm for 5 minutes.

The supernatant will be the rest of the serum lipoproteins with Lp(a) removed. The supernatant is then transferred to a 10,000 molecular weight cutoff filter (Micron

YM-10, Millipore, Bedford, MA), and ultrafiltered in duplicate for 8 minutes at 10,000 rpm in a table top centrifuge. After each filtration, the volume removed from the filter top is replaced with the chosen density gradient the sample is intended to be separated in. The Lp(a) depleted serum sample is recovered from the filter by inversion of the filter top into a 1.5 mL ependorf tube and is centrifuged out via a table top centrifuge at 10,000 rpm for 10 minutes. This Lp(a) depleted sample is then subjected to normal lipoprotein density profiling.

Lp(a) Recovery From Lp(a)-WGA Complex

The sedimented Lp(a)-WGA complex is re-suspended with 150 uL of PBS-p and subjected to filtration with a 45 μm cutoff filter (Ultrafree-MC 0.45, Millipore, Bedford, MA). The transfer tube is washed with 150 uL of PBS-g and the suspended components are discarded into the filter top to ensure that all Lp(a)-WGA complex is transferred. The filter top is washed and filtered one more time with 150 uL aliquots of PBS-p. Then, the filter top is placed onto a new 1.5 mL eppendorf tube and is mixed with 300 uL of PBS-200 mM N-acetyl-D-glucosamine (PBS-g) and is incubated for 30 minutes at room temperature on the orbital shaker. After incubation, the filter top is centrifuged at 6000 rpm for 90 seconds and the filtered solution containing recovered Lp(a) in excess PBS-g is collected. The excess PBS-g is filtered from the sample via a 100,000 molecular weight cutoff filter (Microcon YM-10, Millipore, Bedford, MA) centrifuged at 6000 rpm until the original volume has been replaced 2.5 times by the gradient the sample will be spun in. This sample is then subjected to density profiling identical to the Lp(a) depleted serum sample.

RESULTS AND DISCUSSION

Feasibility of Micro Ultracentrifugation

Currently, the Beckman Optima TLX centrifuge is used to spin ten samples at a time at 120,000 rpms. The minimal throughput greatly inhibits our lab's procedures becoming common place research in clinical laboratories. The small number of samples that can be produced in a normal work day is not very cost effective for clinical physicians and if sample throughput could be increased to at least fifty samples per spin, clinicians could justify the entire procedure and incorporate it into everyday life. With increased clinical efficiency being the prime target, it was decided to attempt a feasibility study on producing a high throughput ultracentrifuge deemed as a μ-ultracentrifuge due to the very small sample volumes.

It was initially decided that utilizing capillary tubes that are mass produced and very in expensive would be the most cost effective route for designing high a high throughput ultracentrifuge. A Delrin® rotor plug was machined to perfectly fit into the existing ultracentrifuge tube slots in side of the Beckman TLA 120.2 rotor. The Texas A&M chemistry machine shop was in charge of all machining needs. Once a number of Delrin® plugs were made, a variety of channels within the plugs could be made to accommodate various capillary tube diameters. Microhematocrit plain capillary tubes purchased from the Fisher catalogue of various diameters were first experimented with. Later, Pyrex® tubing of various diameters was experimented due to the higher modulus of elasticity when compared to silicate glass capillary tubes. Unfortunately, neither capillary tube material would withstand the immense pressures created in an

ultracentrifuge at 120, 000 rpm as all tubes would disintegrate way before gradient formation.

Upon completion of the Microhematocrit capillary and Pyrex® capillary efforts, attempts were directed towards a capillary material that is easily machined and has properties that are easily controlled much like the Beckman polycarbonate tubes. The overall plan was to reproduce the original dimensions of the ultracentrifuge tube with average polycarbonate and proceed to reduce the inner diameter of the chamber until a tiny channel for separations existed. Initially, a plug for the UC rotor was designed that with a single central chamber. See figure14 for a detailed outline of the machined UC tube.

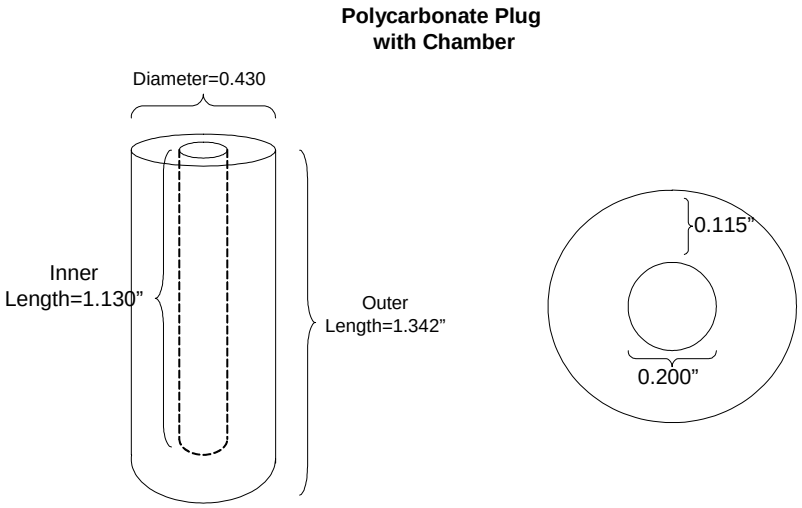

Fig. 14. Chambered plug design for micro-UC experiment.

The final design of the single chambered plug was completed with the intent of allowing a full serum separation at typical operating speeds. The first pair of single

chambered tubes contained a central chamber with an inner diameter (I.D.) of 0.200 inches and a final side-wall width of 0.115 inches

Once machining takes place of any material, optical clarity is compromised by the numerous tooling marks. To solve this dilemma, diluted Methylene Chloride was utilized to restore the optical properties of the Plexiglas as it is a solvent that smoothes out the imperfections in the surface of the plastic. Tests have yet to be conducted that determine whether or not the solvent affects the overall strength of the material, but this is considered to be negligible due to the extent of cleansing with DI H_2O after use.

Since the final tube design will have to withstand 120K rpms for efficient lipoprotein separation, it was decided to immediately spin the new tubes at maximum speed. The chambers were filled with 400 µL of serum/density gradient solution as stated in previous studies. Upon completion of the spin, cracks on the bottom of the tubes were noticeable and allowed a minimal amount of sample to seep out. Even with the small leak on each chamber, a significant amount of banding was achieved. Figure 15 depicts the final results of the slight banding achieved with the chambered plugs compared to a regular UC tube.

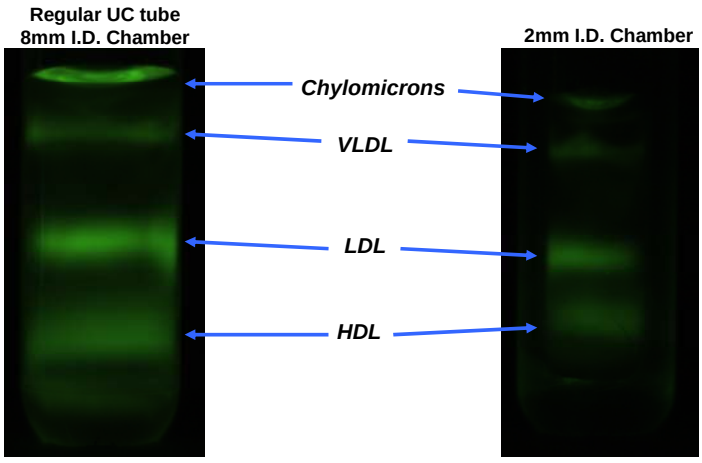

Fig. 15. Micro-UC progression: Comparing standard 8 mm I.D. UC tube to a newly developed 2 mm I.D. UC tube.

By reducing the overall diameter of the ultracentrifuge tubes a rotor will be able to accommodate a larger number of tubes per experiment. In addition to this, the smaller capacity of the ultacentrifuged tubes will require much less gradient and sample volume for analysis. Overall, this should reduce single sample analysis and greatly increase the efficiency and cost effectiveness of the lipoprotein density profiling technique.

Optimization of Rayleigh Scattering Technique

Discovery of Applied Rayleigh Theory

During an attempt to detect oxidized LDL particles through natural fluorescence, detection of lipoprotein particles through light scattering, primarily Rayleigh scattering, was observed. The serum sample was on the order of 60 uL and it was ultacentrifuged in a CsBiEDTA gradient. Due the presence of identical filters on both the emission and excitation sides of the imaging system, Rayleigh scattering was able to be observed. The BG12 filters were used causing a central wavelength of 407 nm to be irradiated on to the lipoprotein particles and since the particles are much smaller than the wavelength, light of wavelength centered on 407 nm was emitted (see figure 16).

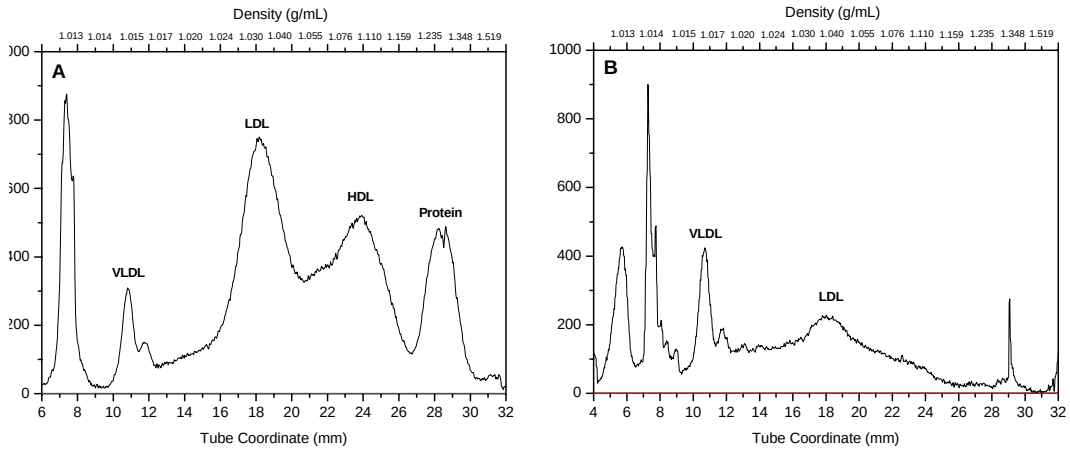

Fig. 16. NBD profile (A) compared to the first observed Rayleigh profile (B).

Figure 16 depicts the normal lipoprotein density profile (A) as well as the assumed Rayleigh scattered profile (B). A normal lipoprotein density profile is achieved by staining the lipoproteins with NBD C_6-Ceramide and imaging the banded classes with a BG12 excitation filter (407 nm) and an OG515 (blocks λ<515 nm). By immediately comparing the two images, it is painfully obvious that the number of peaks in the buoyant portions has increased in the Rayleigh profile and the rest of the peaks in the profile became very convoluted. The camera shutter speed also plays an important role between these two profiles as it is capable of directly increasing intensity as well. The normal profile on the left has a shutter speed of 15.8 mS while the original Rayleigh profile has a shutter speed of nearly one second.

Reviewing the basic Rayleigh scattering theory presented in equation 3, explanation of the profile presented is discovered. The scattered intensity is based upon the incident intensity, one divided by the wavelength of the incident irradiance, and the

diameter of the scattering particle. Since the BG12 filters have a transmittance of 58%, the intensity of the peaks is dramatically lessened form the normal fluorescence profile. The BG12 filters also have a broad transmittance range from 330 nm to 490 nm. This broad range most likely lends itself to scattering interference as non-Rayleigh scattering emission will be detected causing intensity interferences. Although numerous variables have to be understood, the first observance of applied Rayleigh scattering to lipoprotein density profiling shows promise and can not be ignored.

Increasing Rayleigh Intensity

Before any type of quantitation could be attempted, it was necessary to make sure all of the Rayleigh criteria were met. This information can be found in the background section of this thesis. The first order of business was to dramatically increase the Rayleigh signal to ensure that true Rayleigh scattering was taking place free from interference. To accomplish this, the amount of serum was increased slightly to a volume of 100 uL to ensure full banding was being formed throughout the gradient as compared to just 60 uL in figure 16. Lesser serum amounts have been known to cause non-uniform banding causing inconsistent band intensities based on the tube's orientation to the incident light source. Figure 17 displays the intensity change achieved by the serum amount increase.

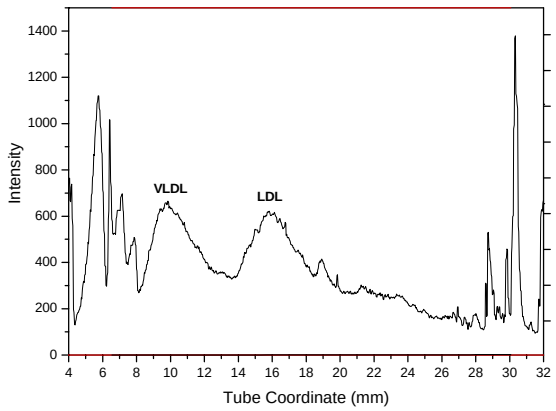

Fig. 17. Increasing Rayleigh scattering intensity by increasing serum amount. 100 uL of serum, 0 uL of NBD, BG12 filters.

Figure 17 shows a decent amount of increased intensity using 100 uL of serum instead of the traditional 60 uL of serum. In addition to the serum volume increase, the profile contains no NBD which was thought to potentially quench scattering intensity at the time of this profile. The LDL peak centered at 16 mm increased by roughly 200 units. Unfortunately, the profile is still very noisy and in need of better intensity still.

The next step in Rayleigh optimization was the use of narrow band pass filters purchased for Edmund optics. These filters have a centered wavelength of 455 nm, a transmittance range from 447 nm to 462 nm, and have a peak transmittance of 52 percent. Since light intensity needs to be increased, the low transmittance of these filters is a drawback. However, the extremely narrow range of wavelength transmitted by the filters is a necessity for accurate quantitation as it prevents any non-Rayleigh related scattering from interfering.

The final optimization with the current Optronics camera and Dolan-Jenner light source was achieved by utilizing an optical slit system with that allows only a specific

amount of light to interact with the sample. All other light is blocked from the camera preventing excess scattering effects. Figure 18 is an example of the increase in intensity achieved by doubling the size of the optical slit used.

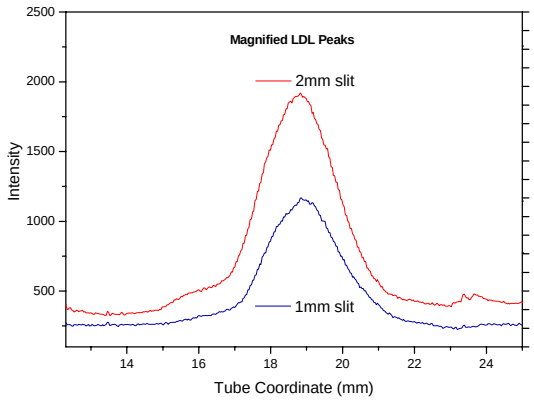

Fig. 18. Increasing Rayleigh scattering intensity: 1 mm optical excitation slit vs a 2 mm optical excitation slit.

Figure 18 shows that doubling the size of the excitation slit will effectively double the amount of incident radiation which in turns doubles the amount of scattered light. Originally, a 0.5 mm slit was used in the initial scattering experiments and the 2 mm slit essentially quadruples the intensity of the novice scattering experiments.

The 2 mm slit is 34 mm in length as to cover the full length of a UC tube and it is positioned exactly 13.87 mm away from the excitation face of the UC tube. Figure 19 gives a representation of the dimensions.

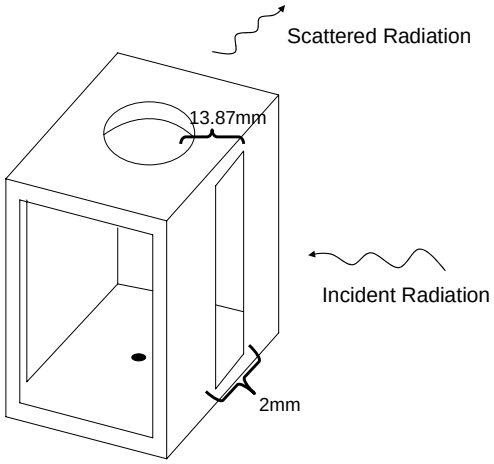

Fig. 19. Sketched representation of optical 2 mm slit orientation and dimensions.

As the light passes through the slit, it experiences Fresnel single slit diffraction due to the close proximity of the image plane. Although some cases can be treated in a reasonable empirical and graphical manner to explain some observed phenomena, the math behind Fresnel diffraction is very complex. I estimated the angles of diffraction by placing a a vertical plane in place of the UC tube and simply measured the width of the incident light on the image plane and calculated the estimated angle of diffraction through simple geometrics. The incident radiation is diffracted at an estimated angle of 18 degrees causing the intense beam of light to interact with the UC tube at a width of about 8mm. 8mm is the exact width of the inner diameter of the UC tube an is ideal for the Rayleigh light scattering experiments. A major benefit of having the incident light the exact width of the UC tube is that the perpendicular sides of the tubes will not be over-exposed from the incident radiation causing superfluous optical effects from the microscopic imperfections in the tube wall.

Improving Scattering Clarity: Removing Foreign Debris

The annoying presence of dust particulates in serum samples is magnified under Rayleigh scattering as the large dust particles create a great Mie scattering effect causing incorrect data violating the Rayleigh approximation for small particles. By removing all traces of foreign debris, data should have cleaner baselines and random sharp Mie scattering peaks from the dust particles will be removed. In the journal article "A comparison of LDL size determination using gradient gel electrophoresis and light-scattering methods," which was written by D. O'Neal and colleagues it is reported that serum samples are heavily filtered prior to ultracentrifugation [67].

Utilizing filters currently stocked with in our laboratory, a filter was that appeared satisfied the criteria of the investigation as well as the criteria of the previously mentioned journal article. I used a Corning syringe filter that measured 13mm in diameter and had an effective pore size of 0.20 microns. This filter is also noted as having a very low protein binding and can handle over 1mL of volume.

In figure 20, the profile and image are of serum solution dispensed in the regular fashion via a pipetteman into a UC tube pulled directly out of the shipping box. This technique is the normal one used in this type of procedure.

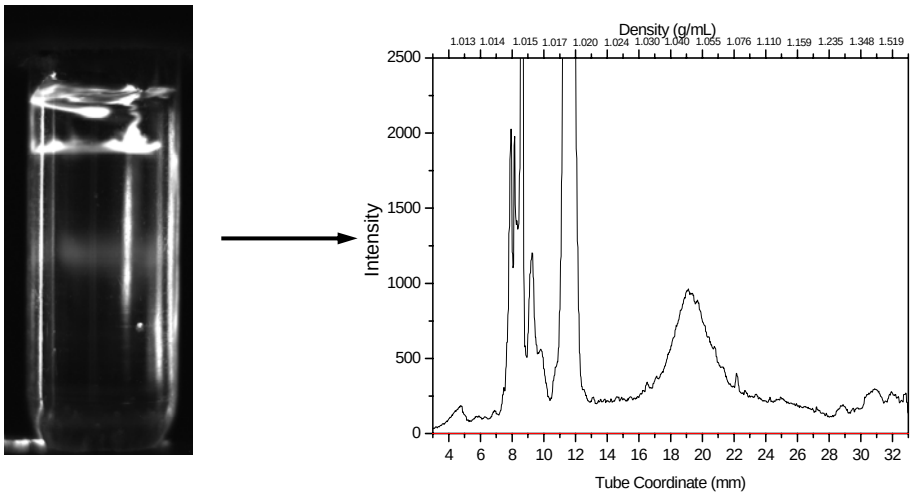

Fig. 20. Example of unfiltered serum sample under Rayleigh scattering conditions.

It can be seen from the image on the left, there is a large dust particle in the lower right portion of the tube. Unfortunately, the images of the tubes do not clearly depict the graphic nature of the dust blemishes as there were numerous smaller particles suspended throughout the tube. The profile more accurately depicts the interference dust particles can make as it shows two of the smaller blemishes located at 22 mm and about 27.3 mm. It is possible that these two blemishes may be mistaken for rare deviations in a patient's serum lipoprotein profile.

Figure 21, displays the same serum sample with the exception that it has been filtered through the corning syringe top filter and dispensed into a DI H_2O rinsed UC tube.

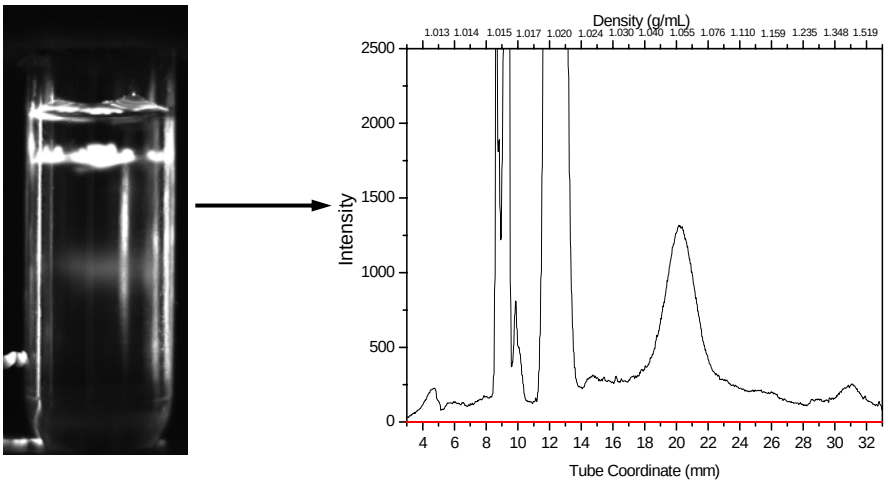

Fig. 21. Example of filtered serum sample and rinsed UC tube under Rayleigh scattering conditions.

The actual image of the UC tube shows no dust particles and it is actually free of minute dust particulates as well. Its profile reinforces what is seen in the tube image as the blemishes in the profile at points 22 mm and 27.3 mm are nonexistent. It should be noted that care must be taken in rinsing the UC tubes as drying with paper products can reintroduce foreign debris. Air drying is preferred.

Qualitative Rayleigh Analysis of Serum Profiles

Lipoprotein Candidates for Rayleigh Analysis

Due to the strict criteria associated with Rayleigh scattering theory, not all lipoproteins make good candidates for the analysis described within this thesis. Full details of Rayleigh criteria can be found in the introduction sections. The scope of this thesis pertains to the scattering of lipoprotein particles fitting in the large lipoprotein classification known as LDL, and there are good reasons for this.

Chylomicrons and VLDL. First and foremost, Chylomicron particles have reported diameters within the range of 80 nm – 1200 nm, and VLDL particles have a diameter range of 30 nm – 80 nm. Their large diameters violate the foundation principle of the Rayleigh scattering theory which dictates that the particle must have a diameter that is much smaller than the incident wavelength of light. A rule of thumb is that the diameter must be less than the λ in nanometers divided by 10 [44]. Since the optimized Rayleigh scattering imaging system utilizes a low transmittance 455 nm wavelength excitation filter, a maximum particle diameter is roughly 45.5 nm. Chylomicron particles and VLDL particles both violate the Rayleigh scattering criteria with our current Rayleigh setup and would require Mie scattering programs to calculate the particle diameters if deemed necessary.

In addition to the Rayleigh criteria, there is an inherent problem with the protocol for density profiling and image analysis. After an ultracentrifugation spin, the chylomicrons and VLDL portions are both banded at the very top of the tube due to both classifications having particles with a density less than the least dense portion of the density gradient. To separate these two classes, a volume of 150 uL of DI H_2O is layered on top of the ultracentrifuged sample. It has recently become evident that this layering technique not only separates the two classes, but it prevents all quantitation of the two types of particles due to band disruptions. Figure 22 accurately depicts the negative results of sample layering.

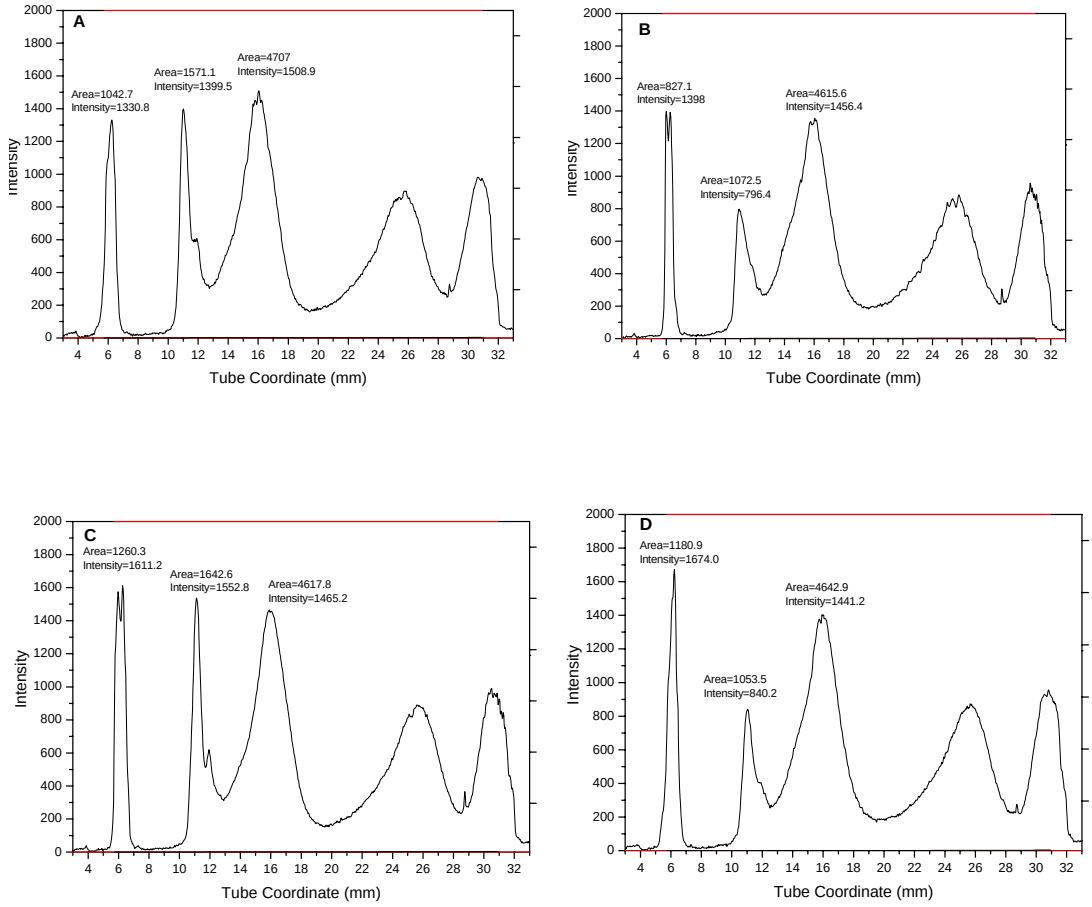

Fig. 22. NBD imaged ultracentrifuged serum sample in $Cs_2CdEDTA$ gradient. Image A is of the tube in the normal imaging position. Images B-D are of the tube rotated 90^o, 180^o, and 270^o respectively from its original orientation.

From analyzing figure 22, the difficulties of quantifying the chylomicron and VLDL peaks can be extremely difficult due to the heterogeneous bands created by layering. The chylomicron intensities vary by as much as 343.2 intensity units and the VLDL peak varies by as much as 756.4 intensity units. The LDL and HDL bands are much more robust as their peaks fluctuate a maximum of 50 intensity units throughout the axis of rotation. Although data for only one serum sample is present, the outcome is identical for all samples. It appears that the less amount of serum used will result in more

drastic changes as the thinner lipoprotein bands are more susceptible to discombobulation.

LDL. LDL is perfect for Rayleigh analysis after isopycnic density profiling because of its size range and importance to atherosclotic risk factors. LDL is reported to have a diameter ranging from 18 nm – 30 nm by most accounts and this diameter range satisfies the Rayleigh scattering criteria. In addition to the size parameter, it was previously stated that the scattering particles need to be single scatterers and must scatter light in an independent manner. Testing for independent and dependent can be simply accomplished by analyzing two samples of doubling concentrations and analyzing intensity increases. If independent scattering is taking place, doubling the particle concentration will result in doubling the overall peak intensity. For example, figure 23 depicts the scattering images of a sample containing 100 uL of serum and an image of a sample containing 200 uL of serum.

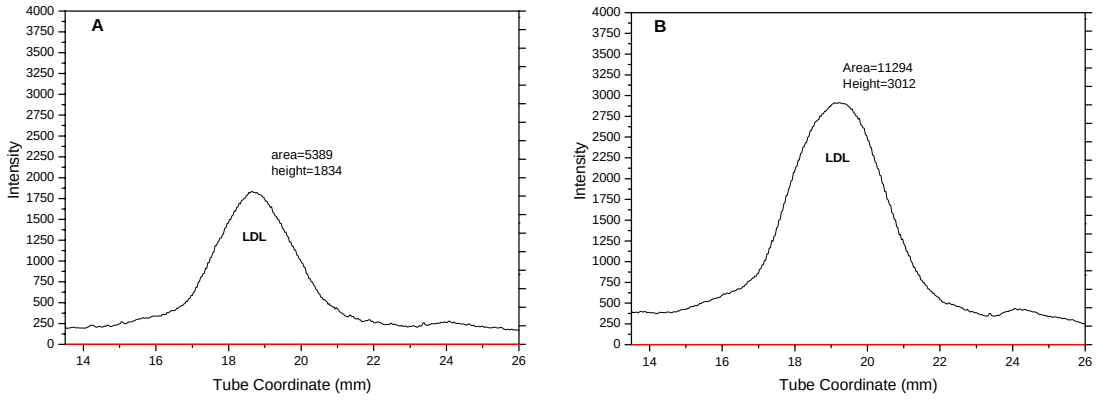

Fig. 23. Independent vs dependent Rayleigh scattering. A and B are magnified density profile LDL peaks from the same serum sample. A contains 100 uL of serum, B contains 200 uL of serum.

The peak intensities do not truly represent the overall increase in the intensity emitted by the LDL class since the larger amount of serum will cause the LDL band to increase in width as well. The area of the peaks is much more informative on the subject of independent versus dependent scattering. From the images displayed in figure 23, the total area of intensity emitted between the two peaks does in fact double as concentration doubles, confirming independent scattering.

HDL. The HDL band in serum profiles has appeared to be too small and very difficult to detect with our current imaging system. The reported diameter range of HDL particles starts as low as 5 nm and peaks at 13 nm. The intensity of light emitted from a particle due to Rayleigh scattering is immensely dependent upon its effective diameter as the diameter is raised to the sixth power in the theory calculations. This means that the average HDL diameter of roughly 9nm has a scattering intensity that is more than 400 times less than that of the average LDL particle of 24.5 nm both being the same concentration. The outcome of the poor intensity emitted by the HDL particle results in no detected HDL particles. The following figure represents this negative characteristic of our imaging setup.

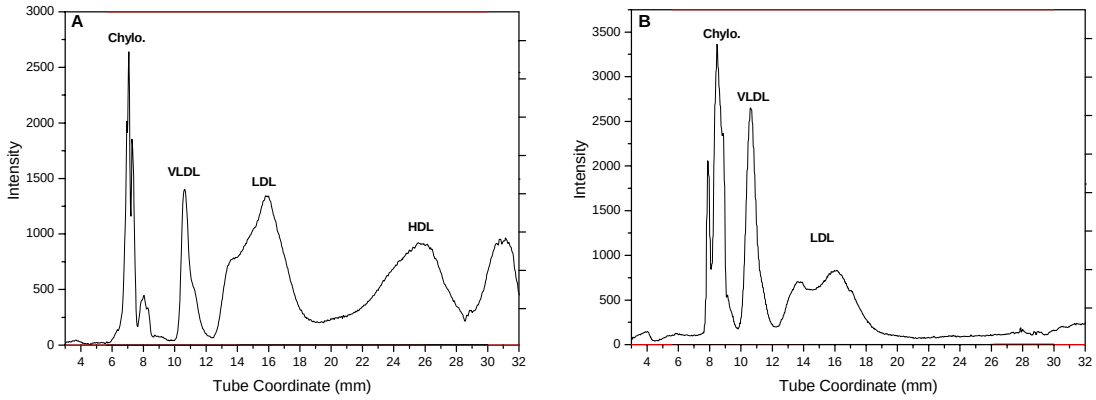

Fig. 24. Comparative slides of an NBD stained profile versus a non stained Rayleigh profile. A is a NBD profile with 100 uL of serum stained with 4 uL of NBD separated in a Cs_2CdEDTA gradient. B is a Rayleigh profile with 100 uL of serum separated in a Cs_2CdEDTA gradient.

Figure 24 compares a typical NBD serum profile (A) and a Rayleigh scattering serum profile (B). Both serum samples depicted in the images are from the same patient and blood draw date. In the image, it is very clear that the small diameter of the HDL causes it to not be detected by means of Rayleigh scattering. However, the HDL class is very much present as seen in the NBD profile in image A. Initially, the loss of HDL data apparent with Rayleigh scattering could be viewed as a major drawback, but there is actually a very positive aspect to this characteristic. Lp(a) is deemed as a risk factor for atherosclerosis, and this particular particle can be easily detected by Rayleigh scattering due to the absence of the HDL Rayleigh peak.

Lp(a). Lp(a) coincidentally has a density range that overlaps with small dense low density lipoproteins as well as the large less dense high density lipoproteins. Table 1 lists all major lipoprotein classifications and their respective densities. Lp(a) is reported to have a density range of 1.050-1.100. Intuition would lead one to believe that Lp(a)

will most likely be hidden in the tailing peak of LDL as well as the starting peak of HDL if particle concentrations are similar. However, the Lp(a) diameter range starts at 25 nm and ends at 35 nm. With very small dense LDL ranging from 15 nm to 20 nm and large HDL particles ranging from 10 nm to 13 nm, the large Lp(a) particle can be easily discerned in a Rayleigh scattering profile if it is present in a reasonable amount. Figure 25 is an example of Lp(a) detection via Rayleigh scattering.

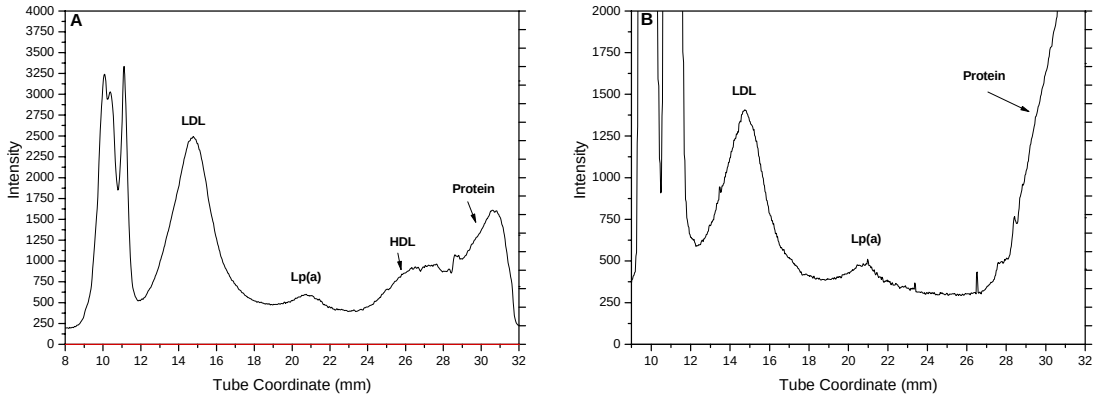

Fig. 25. Comparative NBD profile (A) and Rayleigh profile (B) of identical serum samples containing Lp(a).

The serum sample depicted in figure 25 actually has very minimal amounts of small dense LDL and large less dense HDL particles, but it acceptably illustrates a serum sample containing Lp(a). This image is solid proof that a minimal amount of Lp(a) can be detected in Rayleigh scattering. Furthermore, it is possible to detect Lp(a) in serum samples that contain ample HDL masking the Lp(s) peak. Under Rayleigh imaging, the HDL peak will essentially disappear exposing the large diameter Lp(a) particles. Therefore, Rayleigh scattering can be used as a simple diagnostic tool for determining hidden Lp(a) particles in banded samples prior to further analysis.

Serum Profile Analysis of Three Samples

For qualitatively analyzing serum density profiles, the $Na_2CdEDTA$ gradient was chosen. This gradient was chosen as it significantly spreads out the LDL and Lp(a) regions of the profile. Both of the regions' Rayleigh scattering as well as medical benefits have been previously described. By spreading out the LDL band, the HDL and protein sections of the profile are joined as the gradient does not reach the appropriate density to separate the two classes. You will notice in the following profiles, the HDL and protein essentially settle at the bottom of the tube.

In order to qualitatively analyze serum profiles, one first must make a few assumptions for comparisons sake as well as take into account the expected serum profile trend based on the Rayleigh approximation. The first assumption is that all particles are of identical concentrations throughout the particle diameter range. The second assumption to be made is that the particle diameter of LDL decreases as density of the gradient increases. This means that going from left to right in the LDL band will allow one to see a drop in particle intensity. With these assumptions being made, a crude intensity curve throughout the LDL band can be constructed. Figure 26 is an example of the Rayleigh calculated particle intensities based on particle diameters while all particles are of equal concentrations.

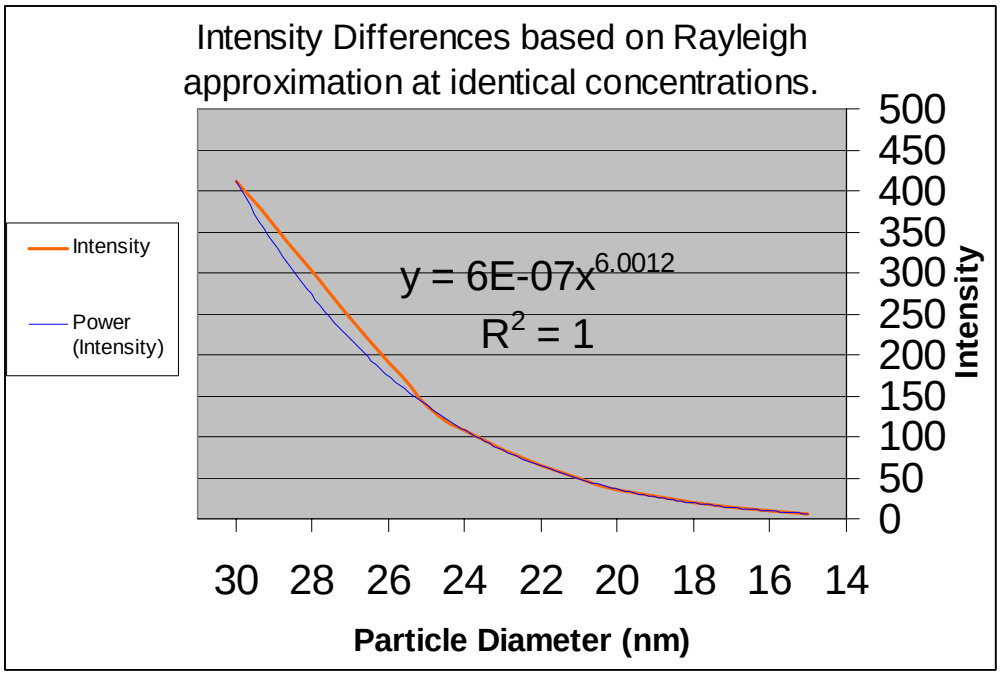

Fig. 26. Rayleigh scattering intensity curve emitted by varying diameter sizes at equal particle concentrations.

Essentially, the calculated line of best fit on the graph will give the researcher a curve of reference to compare to the intensity peaks emitted by the LDL and Lp(a) bands. Taking the assumptions into consideration, any deviations from the intensity curve will relate to changes in relative particle concentrations. Three different serum samples will be qualitatively analyzed by this means in the following portion of this thesis.

Sample 1. The first sample to be qualitatively analyzed within this thesis is Figure 27, and it is of a normolipidemic patient and it compares the LDL peaks of a stained 100 uL sample of serum imaged under NBD settings, and a non-stained 100 uL serum sample imaged under Rayleigh settings.

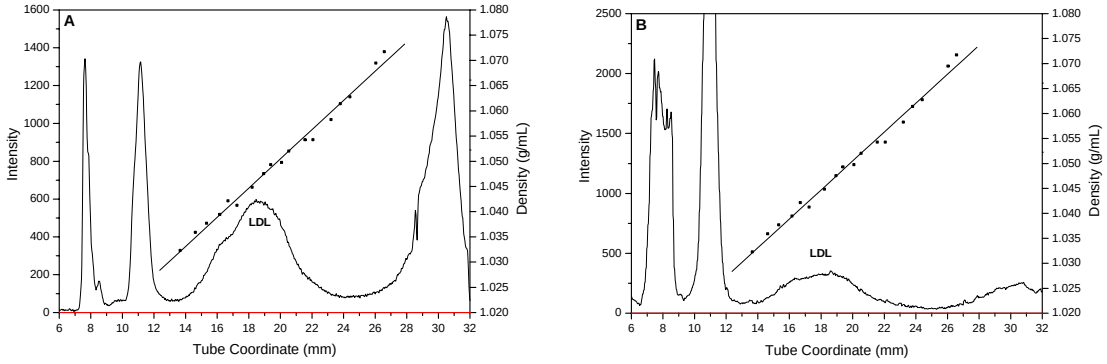

Fig. 27. Profile comparison of 100 uL serum samples with two prevalent LDL subclasses. (A) is an NBD stained 100 uL serum sample and (B) is a non-stained 100 uL serum sample.

In NBD profile A of Figure 27, particle concentration can be loosely associated with the peak heights and peak areas since the intensity can be correlated to the number of NBD fluorophores in fluorescent domains. The number of NBD fluorophores can then be correlated to amount of serum particles as the fluorophores will only fluoresce when imbedded in a fluorescent domain, such as a lipoprotein particle. The LDL peak appears to be of a significant concentration level and there is a definite presence of two types of LDL. At a tube coordinate of 17 mm there is a shoulder suggesting that two types of LDL may be present. The Rayleigh scattering profile depicted in B of figure 27 would suggest that the average particle diameter of the first peak (14 mm - 17 mm) would be larger than the particle diameter of the second type of LDL (17 mm - 24 mm). This prediction is confirmed by particle sizing data obtained on the two excised lipoprotein fractions and is presented in figure 28.

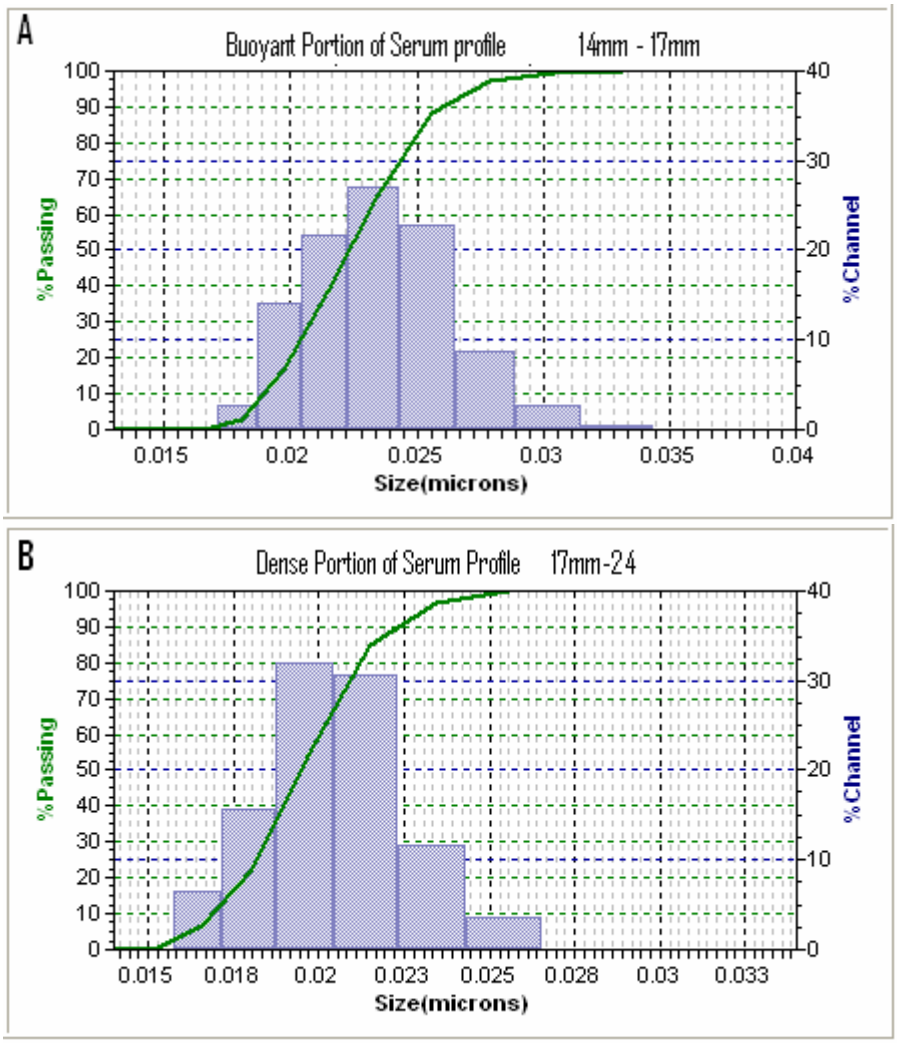

Fig. 28. Microtrac Nanotrac particle sizing data of the buoyant portion (A) and the dense portion (B) of the profiles depicted in figure 27.

Figure 28 shows the average particle diameter present in the buoyant fraction (14 mm – 17 mm) to be 24 nm. The average diameter of the dense LDL portion (17 mm - 24 mm) is 18 nm. The large diameter ranges present in the particle sizing data is a result of the presence of VLDL and dense LDL subclass in the buoyant fraction, and buoyant LDL subclass in the dense fraction. This occurs because the method used to excise the fractions has a error range up to one millimeter in length. This allows small portions of

overlapping serum fractions to be included in each analysis. This trend is present throughout the particle sizing data.

Rayleigh Image B of figure 27 confirms the significant presence of LDL; however, a slightly contrasting story is presented. Taking into consideration the intensity curve presented in figure 26 and assuming that LDL particle diameter is largest at a tube coordinate of 14 mm and smallest at a tube coordinate of 24 mm, insight to particle concentrations can be achieved. The second LDL peak at 19 mm should, in theory, be smaller than the larger diameter peak found between 14 mm and 17 mm, but it is in fact larger. This indicates that the smaller diameter peak after 17 mm actually has a much larger concentration than the larger diameter particles. This determination is confirmed in further analysis utilizing an Apo B-100 specific concentration determination kit. For an excised fraction of the buoyant LDL particles corresponding to the range of 15 mm to 16.5 mm on the NBD profile in figure 27, an Apo B100 concentration of 14.04 mg/dL. The excised fraction of the dense portion corresponding to the range of 18mm to 19.5 mm on the NBD profile in figure 27 has a concentration of 21.05 mg/dL. Due to the inconsistency of the excision method, these concentration values can not be held as precise, but nonetheless the values do prove the Rayleigh qualitative data in that the dense portion has a higher LDL concentration that that of the buoyant LDL portion.

*Sample 2***.** The second serum sample to be analyzed is of a patient containing large concentrations of three prevalent LDL subclasses. Figure 29 pictures both the NBD profile (A) and the Rayleigh scattered profile (B) of the same serum sample.

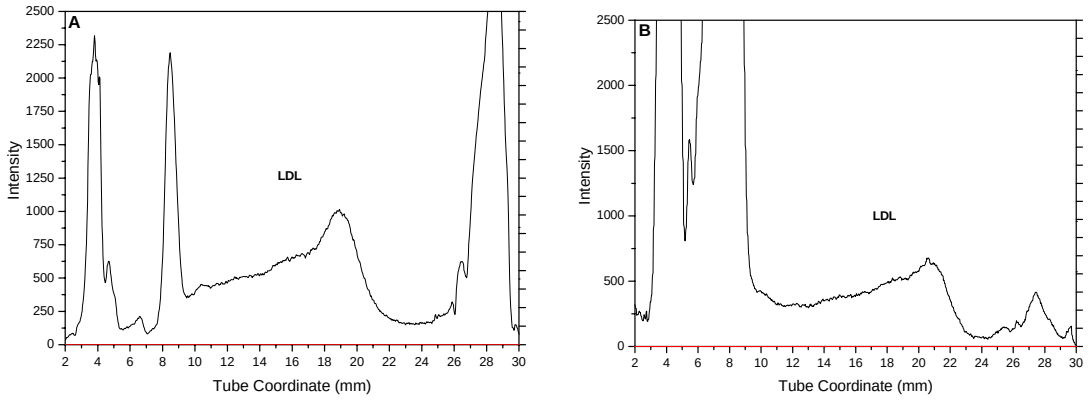

Fig. 29. Profile comparison of 100 uL serum samples with three prevalent LDL subclasses. (A) is an NBD stained 100 uL serum sample and (B) is a non-stained 100 uL serum sample.

NBD profile A in figure 29 shows a very broad LDL band that has three subclasses present. The first subclass is called the buoyant portion and ranges from 10 mm to 14.5 mm. The second LDL subclass will be referred to as the middle subclass and it ranges from 14.5 mm to 17.5 mm. The third and final LDL subclass will be referred to as the dense portion ranges from 17.5 mm to 23 mm. Since the entire classification of LDL particles ranges from 15 nm to 25 nm, it is assumed that the buoyant subclass is larger than the middle subclass and the dense subclass has the smallest diameter of the three. Particle sizing data obtained from the Microtrac Nanotrac 250 is offered in figure 30. The particle sizing data confirms the assumptions of the particle diameter by reporting the buoyant portion to have an average diameter of 27 nm, the middle portion to have an average diameter of 23 nm, and the dense portion to have an average diameter of 19 nm.

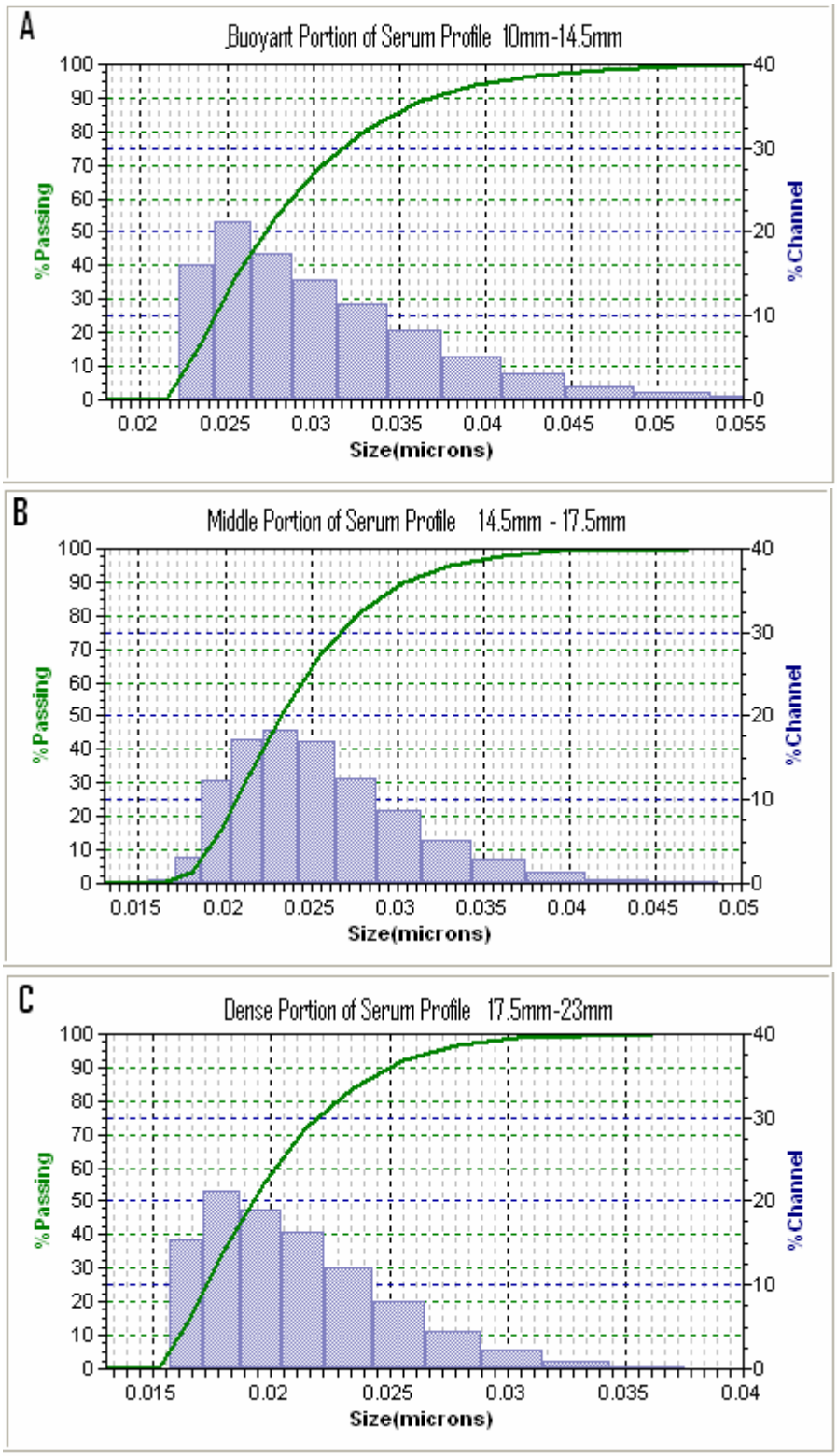

Fig. 30. Microtrac Nanotrac particle sizing data of the buoyant portion (A) and the dense portion (B) of the profiles depicted in figure 29.

In addition to the particle diameter data, Apo B-100 concentration data was also obtained on the three excised sample. From analyzing the Rayleigh profile in figure 29 and comparing it to the intensity curve determined in figure 26, the dense portion of the broad LDL peak should be of a concentration significantly more than the other two LDL fractions. To determine relative concentrations, fractions were excised from the tubes using the NBD profile as a template. 11 mm to 12.5 nm was used a the buoyant fraction, 14.5 mm to 16 mm was used as the middle fraction, and 18 mm to 19.5 mm was used as the dense fraction. The data obtained on LDL concentration shows the buoyant fraction to have a concentration of 17.39 mg/dL, the middle fraction to have a concentration of 23.91 mg/dL, and the dense portion to have a concentration of 34.78 mg/dL. This data once again proves the estimations made based on the Rayleigh scattering profile.

Sample 3. The third serum sample chosen to be evaluated by means of Rayleigh scattering data is a sample that contains two distinct LDL subfractions as well as a significant amount of Lp(a). The sample is known to contain the Lp(a) particle from Lp(a) differential density profiling analysis performed by both Leticia Espinosa and Sarah Tillford from the Laboratory of Cardiovascular Research. Figure 31 displays the NBD profile (A) of this serum sample as well as the Rayleigh scattering profile (B) of the serum sample.

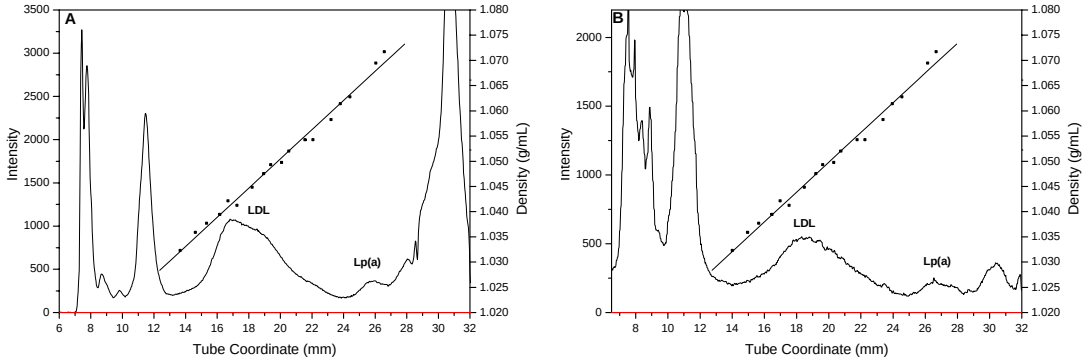

Fig. 31. Profile comparison of 100 uL serum samples with two prevalent LDL subclasses as well as a Lp(a) band. (A) is an NBD stained 100 uL serum sample and (B) is a non-stained 100 uL serum sample.

NBD profile A in figure 31 shows two distinct LDL classes with a minor separation between the two peaks at 18 mm. The first peak starts at 14 mm and ends at 18 mm while the second peak starts at 18 mm and ends at 23 mm. The NBD profile also depicts a significant Lp(a) peak at 26 mm. The Rayleigh profile (B) depicts the LDL band to be of the same width, but the resolution between the two separate peaks lost due to concentration levels. However, the particle sizing data obtained for the first two LDL peaks as well as the Lp(a) fraction are pictured in figure 32.

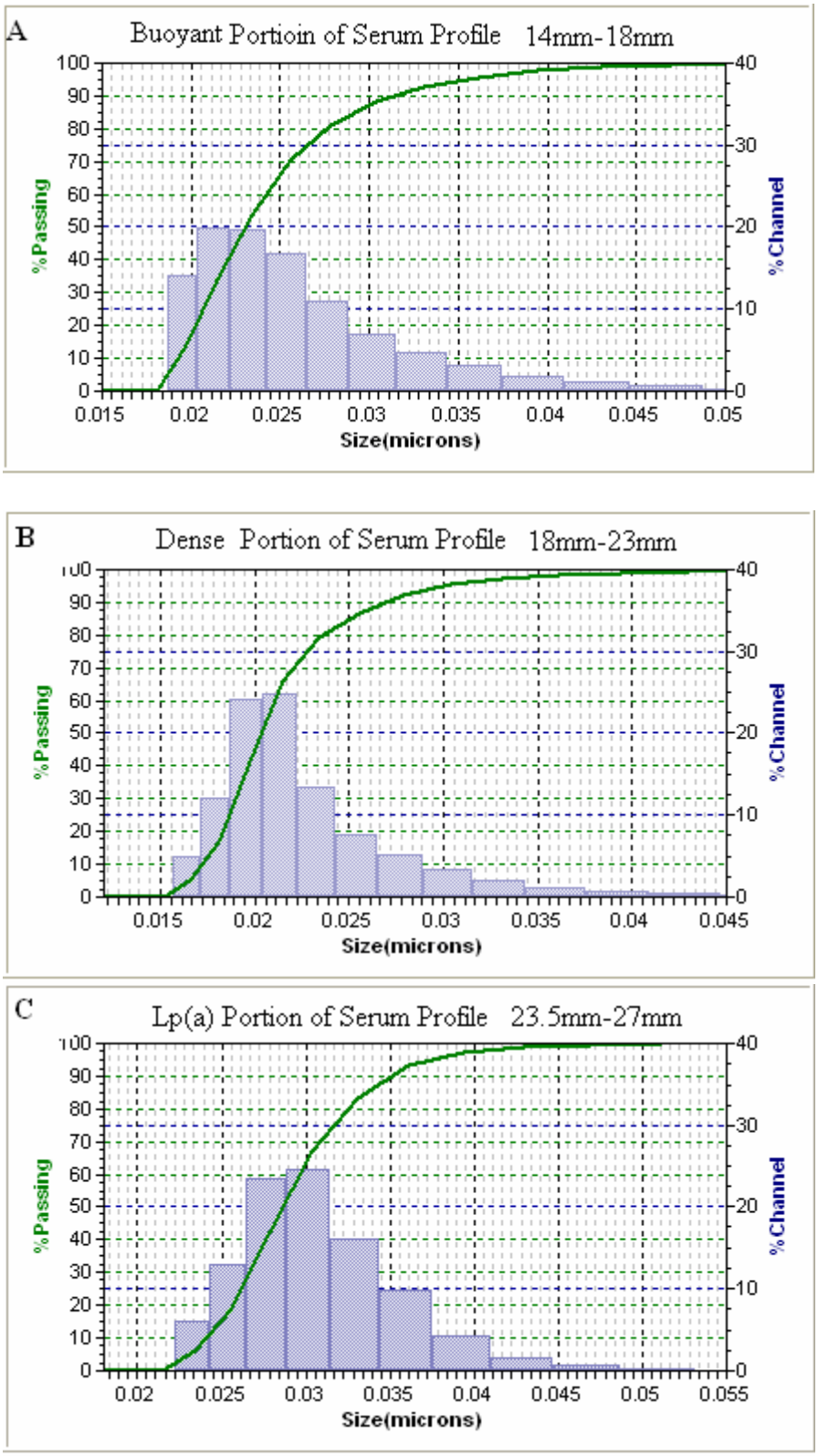

Fig. 32. Microtrac Nanotrac particle sizing data of the buoyant portion (A), dense portion (B), and Lp(a) portion of the profiles depicted in figure 31.

The data obtained from figure 32 states that the average diameter of particles in the buoyant fraction is 23 nm, 20 nm in the dense fraction, and 29 nm in the Lp(a) fraction. This data confirms the Rayleigh assumptions on particle diameters throughout the LDL band for a third time. In addition to the particle sizing data, only qualitative estimations of particle concentrations can be made as this particular serum sample was no in abundance preventing Apo B-100 concentration determinations. From the NBD profile one can loosely assume that the first detected LDL peak is of higher concentration that that of the second LDL peak. By comparing the Rayleigh peak to that of the intensity curve, the concentrations of particles across the LDL band appear to be relatively uniform.

Possible Quantitation via Rayleigh Scattering

Currently, Rayleigh scattering is primarily qualitative information and can be used in conjunction with the NBD profiling to obtain true estimations of lipoprotein concentration within the various LDL subclasses as well as Lp(a). In order for quantitative results from scattering to exist, the researcher must be left with just one unknown in the Rayleigh equation. Take into account the Rayleigh scattering equation based on the particle's cross section in equation 25.

$$\sigma_s = [(2\pi^5 d^6 n_{med}^4 / 3\lambda^4) * (n^2\text{-}1 / n^2\text{+}2)^2] \quad (25)$$

Relating equation 8 to equation 25, the particle concentration can be calculated. This relation is seen in equation 26.

$$\rho = \ln(I_s/I_o) / (- \sigma_s R) \quad (26)$$

The symbol ρ in equation 26 actually represents particle concentration although it is sometimes referred to as particle number density. This is explained in the works of A. J. cox [48]. Full explanation of these two formulas can be found in the Rayleigh scattering section of this thesis. From the two equations, the two unknowns are the diameter of the particle and the particle concentration. However, it is conceived that particle diameter can be related to particle density as particles with a specific diameter have a specific density. Once a large enough sample of patients have had there serum analyzed, a chart denoting the particle diameter to be expected at a given density should be able to be constructed.

Before this calculation can be utilized in our system, it would be wise to run data on solutions with known particle diameters as well as concentrations. By doing this, calculated concentrations can be compared to similar known concentrations, and any differences may lead to a normalizing factor for our system. To complete this task, NIST size standards purchased from Duke Scientific were employed as well as size standards from Invitrogen. The size standards chosen were the 30 nm Duke spheres as well as the 20 nm Invitrogen spheres. Figure 33 shows the Scattering profiles of Invitrogen 20 nm standards in image A and Duke nanospheres in image B.

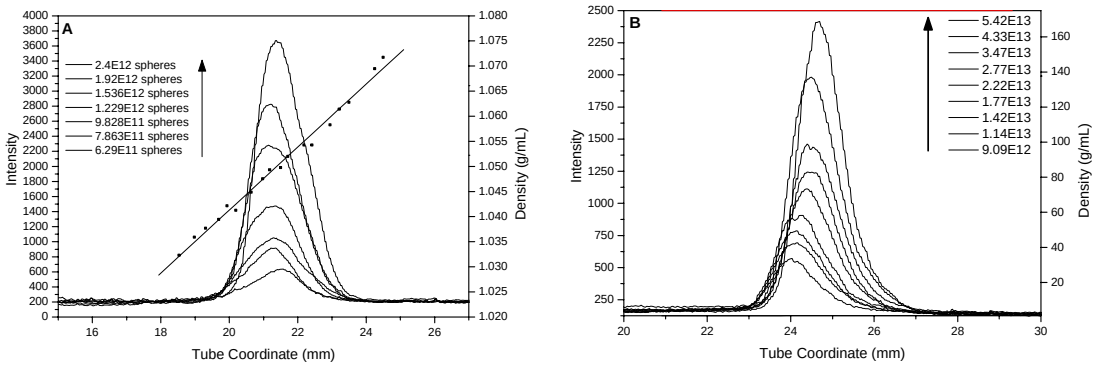

Fig. 33. Size standard profiles at varying concentrations. A is the 20 nm Invitrogen size standards and B is the 30 nm Duke size standards. Concentrations noted as particles per milliliter.

Both graphs of the size standards portrayed in figure 33 show a linear relationship between particle concentration and intensity. Intuitively, this data is accurate as one would expect the intensity to double as concentration doubles within a specified particle diameter. Although the principle behind the quantitation step is valid, it has yet to come to fruition due to hindrances using particle standards within the EDTA salt gradients.

Errors in the size standards' diameters where discovered under Microtrac particle determinations. To fully illustrate this problem, particle sizing graphs of the 20 nm Invitrogen spheres diluted in a $Na_2CdEDTA$ gradient are presented at varying concentrations in figure 34.

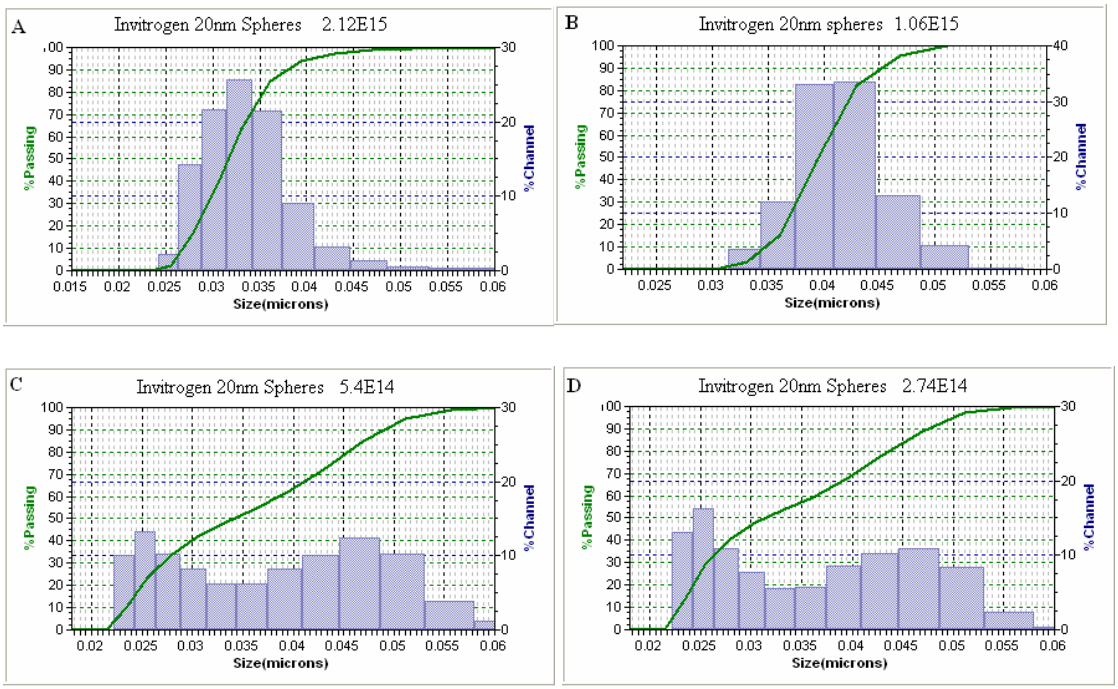

Fig. 34. Microtrac Nanotrac particle sizing data for Invitrogen 20 nm spheres at decreasing concentrations. Concentrations noted as particles per milliliter.

Figure 34 depicts the measured particle sizes for the Invitrogen 20 nm spheres at decreasing concentrations. Graph A is of the highest concentration while D is the most dilute sample. It can be deduced from the graphs that a degree of flocculation occurs amongst the particles as they become more and more dilute. The lessening of particle surfactant between solutions as well as decreasing Debye lengths due to the high ionic strength of the gradient is most likely the explanation for the observed data. Thankfully lipoproteins are not as susceptible to this phenomenon like the particle standards. However, it is crucial to overcome this drawback if quantitation using applied Rayleigh theory is pursued with the current camera system. For quantitation purposes, size standards will have to be reduced to a concentration near 8.73E13 particles per mL as this is the average LDL concentration for an average serum sample [8].

Use of Alternate Light Sources for Rayleigh Scattering

In exploring Rayleigh theory within our camera system, it has become evident that incident light intensity must be maximized for best resolution and detection of particles. In addition to this, it is also crucial to have the incident radiation be a specific and narrow wavelength in order to prevent multiple scattering and other scattering interferences associated with wide ranges of wavelengths. One alternative light source to be used in Rayleigh scattering is that of a laser light source.

Laser Technology

Lasers have been around for decades and are typically part of any analytical chemistry instrument at some level. The word Laser is actually an acronym for "Light Amplification by Stimulated Emission of Radiation." Nonetheless, they are highly selected for their very intense and highly collimated beams that operate at lower milliwatt power ranges. A common laser choice is one based on a solid crystalline material as the lasing medium. Optically pumping is the process of depopulating one state of an element to another using high power infrared electromagnetic radiation. Typical elements used are rubidium crystals (Rb) or a doped form of yttrium aluminum garnet (YAG) material. Unfortunately, the power lasing beam produced of such materials is in the infrared range and usually on many accounts as it is invisible. Since material costs tend to increase significantly as emitted laser wavelengths decrease, a cost effective choice is to frequently use a laser in the infrared range and internally multiply the wavelength allowing a shorter wavelength to be emitted.

Wavelength multiplication can be achieved by passing the pumped beam through another crystal medium that responds in a nonlinear way to the infrared radiation. By doing this, frequency components emitted will be of multiples or harmonics of the original beam of radiation [68]. When potassium titanyl phosphate crystal lattices are used in conjunction with an intense infrared beam of wavelength 1064 nm, the output will be of the second harmonic of the original resulting in a wavelength of 532 nm [69]. This wavelength corresponds to intense green light highly visible to the naked eye as well as camera based on a three CCD (charge coupled device) system.

A classIIIa laser produced by OnPoint Lasers is employed for image analysis research and development by our laboratory as it is inexpensive and met the requirements of our needs soundly. The 532 nm wavelength emitted is highly collimated meaning that it has essentially no beam divergence unlike our metal-halide lamp. The wavelength in the green portion of the spectrum is well detected by both the camera as well as the human eye. Being able to easily see the laser through the samples makes geometric adjustments a breeze.

A wavelength of 532 nm will also omit the use of an excitation filter causing the detected intensity to be lessened by only the scattering emission filter place on the camera lens. This in itself will double the intensity currently seen in the current system independent of incident intensity since we currently utilize a double optical filter setup. Although scattering light emitted from a diode pumped solid state laser is groundbreaking technology in our procedures, conclusive results proving the attributes of a laser source have been obtained.

Laser Rayleigh Scattering

Using a 100 uL sample of serum has been depicted throughout this thesis as producing detailed information about the LDL and Lp(a) classes of lipoproteins. However, a recent change in protocol to 6 uL samples stained in NBD has been utilized for clinical analysis. At such a small serum volume, enough sensitivity using the current Rayleigh scattering procedure can not be efficiently produced. Thankfully, the 532 nm green laser can provide enough intensity to extract data from portions of samples containing the minute amount of serum. Much like the rest of this thesis and staying true to Rayleigh criteria, the LDL and Lp(a) particles are targeted.

Figure 35 depicts a 6 uL serum sample stained with a saturating amount of NBD of 10 uL. The sample was then ultracentrifuged in a Cs_2CdEDTA gradient and profiled with NBD and green wavelength Rayleigh settings (see Experimental section).

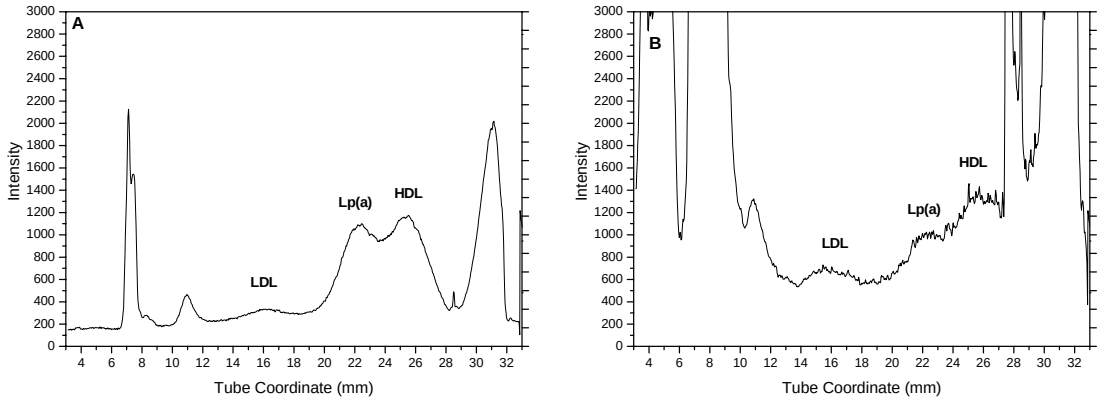

Fig. 35. 6 uL serum sample stained with 10 uL of NBD and imaged with NBD settings (A) and Rayleigh settings (B).

Figure 35 is definitive proof that the 532 nm green laser is a feasible candidate for Rayleigh scattering detection of LDL and Lp(a) particles. The serum sample profiled

does in fact contain Lp(a) and this was previously determined within our laboratory using the labor intensive and costly procedure of differential density profiling outlined in a previous section. However, if the Lp(a) determination was not previously known, a researcher could mistake the peak for a buoyant portion of HDL. There is nothing in the two profiles indicating otherwise as Lp(a) has overlapping densities with both LDL and HDL. In the section "Candidates for Rayleigh Scattering," I mention how scattering of the Lp(a) particle can be detected and discerned from the HDL peak due to its large size and the non-existent scattering effects of the HDL particle. Unfortunately, this is not the case in profile B of figure 35. The HDL peak can be easily detected along with the LDL and Lp(a) peaks. This is most likely due to the saturation of NBD as the 532 nm excitation beam will excite the NBD fluorophore to a small degree causing emission from the fluorophore in the green wavelength. The resulting NBD emission will be detected by the camera as the emission filter used is relatively broad in the green wavelength range.

Figure 36 confirms the interference of the NBD fluorophore as the profiles depicted are of the same serum sample used in figure 35 with the exception of having no lipoprotein stain present.

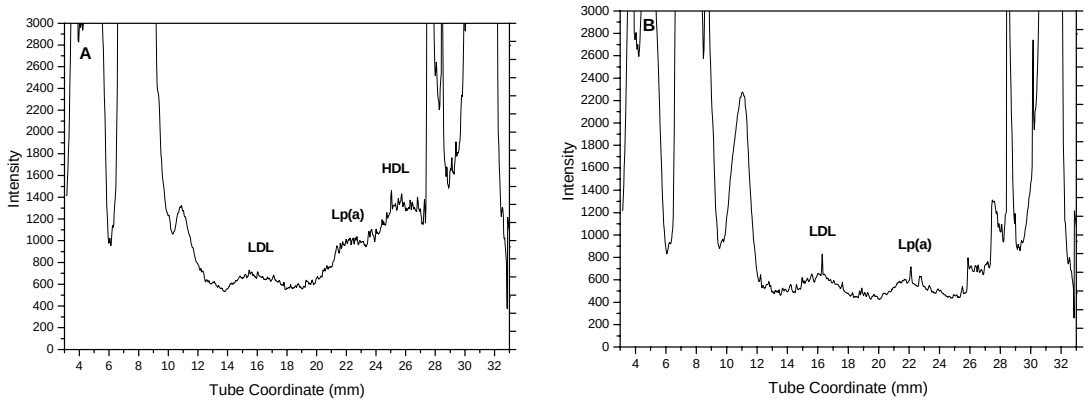

Fig. 36. 6 uL serum sample stained with NBD and Rayleigh imaged (A) compared to the same 6 uL serum sample lacking the NBD stain and profiled with Rayleigh settings (B).

Figure 36 presents data that confirms the influence of NBD within Rayleigh scattering serum profiling. As one can see, profile B in figure 36 shows only the LDL peak and Lp(a) peaks due to the inherent characteristics of the Rayleigh technique previously discussed. By using the green laser, it is feasible to detect the presence of Lp(a) in the ultracentrifuged tube allowing efficient analysis of the lipoproteins bands to follow. By detection of the Lp(a) particle in the ultracentrifuge tube a clinical researcher will know to determine Lp(a) concentrations instead of just testing every sample for concentration and presence at the same time. This technique will undoubtedly save overhead fees for any clinic allowing diagnostic tests to become cheaper.

In addition to the green laser, it may be possible to acquire a diode pumped solid state laser emitting a wavelength of light at 493 +/-3 nm allowing even more sensitivity and intensity to be attained. A diode-pumped Yb-doped tungstate (Yb:KY) laser crystal emitting on its zero phonon line (ZPL) resonance transition at a wavelength about 986 +/-

6 nm, whose fundamental infrared output radiation is harmonically doubled via a non linear crystal resulting in the emitted narrow blue spectrum [70].

CONCLUSION

The overall scope of the research presented in this thesis was governed by the pursuit of feasibility studies that take lipoprotein profiling by ultracentrifugation to a new innovative pedestal. It has been portrayed throughout the history of scientific thought that the most astounding discoveries have been by accident and abstract thought. The data I have presented here is nothing short of a groundbreaking imaging technique applied to ultracentrifuged serum samples that have been developed from a faulted non-related experiment.

The initial heartaches associated with the staining of lipoprotein particles by the fluorophore NBD C_6-Ceramide left much to be desired when quantitation of particles was concerned. As information on lipoprotein uptake by the different lipoprotein classes comes forth at a slow rate, it is conceived that quicker quantitative data could be derived from naturally occurring fluorophores within the lipoproteins. Concentrating on the characteristics of tryptophan, it was initially thought that applying the proper excitation and emission filters, the natural fluorescence of lipoprotein particles could be detected. This attempt at quantitation appeared to fail miserably until a phenomenon derived from identical excitation and emission filters was observed from the serum profile.

By using the filter combination of a 407 nm centered wavelength filter on the excitation and emission sides, a phenomenon better known as Rayleigh scattering was observed. The light scattered off of the lipoproteins was dictated by individual diameters allowing particles with diameters much smaller than the wavelength of incident radiation to have their approximated concentrations calculated by means of the Rayleigh approximation theory. This discovery gives our laboratory much hope that the important

LDL subclasses as well as the Lp(a) subclass can have their concentrations calculated in the absence of a lipoprotein stain.

The Rayleigh scattering theory has been applied to the density profiling technique employed in our laboratory to prove feasibility of the general concept. In solidifying the feasibility aspect, the scattering technique has undergone great strides towards optimization. The amount of serum has been narrowed down to 100 uL as it allows complete lipoprotein banding throughout the dimensions of the tube. An optical 2 mm slit placed 13.87 mm away from the face of the tube in line with the incident radiation source allowed maximum incident radiation for the lipoprotein particles. The use of the optical slit also significantly reduced unwanted scattering interferences decreasing the spectra noise. Using 455 nm narrow band pass filters on the excitation and emission sides of the imaging system provided the most intense and clear scattering spectra, as non-Rayleigh scattering was prevented. The final optimization effort included serum and gradient filtering as well as UC tube rinsing just before subjecting samples to isopycnic separations. The filtering process greatly eliminated the possibility of dust particulates scattering light, causing misleading serum profiles.

Once the optimization of the Rayleigh technique was complete, attention was turned to eliminating one of the unknowns presented within the Rayleigh equation. The unknown easiest to determine by a separate analysis is the particles' diameters due to the overwhelming amount of instrumentation in the scientific field. A Microtrac Nanotrac 250 was utilized for verification of lipoprotein particles. Without a doubt, the data acquired for the Microtrac dynamic light scattering instrument verified the published particle diameters giving hope to potential quantitative concentration efforts. The data

presented proves feasibility for the hypothesis that particle diameters will relate to a specific density with in an isopycnic gradient. With the evolution of the data in the future, lipoprotein concentrations can be determined effortlessly through Rayleigh scattering theory.

The final, but most innovative feasibility undertaken was that of using alternate laser light sources for the scattering of lipoprotein particles. By using a 532 nm wavelength diode pumped solid state laser, tremendous scattering intensity can be achieved. By using a light source of this nature, serum volumes can be drastically decreased to 6 uL. It has been clearly proven that both the LDL class and the Lp(a) class can be detected at a serum volume of 6 uL when the 532 nm green laser is used. The future of using a laser as a Rayleigh light source can have a profound effect on the medical world. With Lp(a) being one of the fore running risk factors attributed to atherosclerosis, immediate detection within the spun UC tube from laser Rayleigh scattering will allow researchers to further analyze the particle efficiently.

REFERENCES

[1] T. Thom, N. Haase, W. Rosamond, V. Howard, J. Rumsfeld, T. Manolio, et al., Heart disease and stroke statistics-2006 Update. Circulation. 113 (2006) e85-e151.

[2] M. H. Beers, ed., The Merck manual of health and aging: atherosclerosis. Merck Research Laboratories, 2005. Merck & Co. Inc. accessed on 6-12-2006 <http://www.merck.com>.

[3] R. Ross, Atherosclerosis- an inflammatory disease. N Engl J Med. 340 (1999) 115-126.

[4] M. A. Crowther, Pathogenesis of atherosclerosis. Hematology. (2005) 436-441.

[5] P. Libby, P. M. Ridker, A. Maseri, Inflammation in atherosclerosis. Circulation. 105 (2002) 1135-1143.

[6] P. C. Choy, Y. L. Siow, D. Mymin, K. O, Lipids and atherosclerosis. Biochem. Cell Biol. 82 (2004) 212-224.

[7] J. L. Witzum, D. Steinberg, Role of oxidized low density lipoprotein in atherogenesis. J. Clin. Invest. 88 (1991) 1785-1792.

[8] N. Rifai, G.R. Warnick, M.H. Dominiczak (Eds.), Handbook of Lipoprotein Testing, ACC Press, Washington, DC, 1997.

[9] R. Carmena, P. Duriez, J-C. Fruchart, Atherogenic lipoprotein particles in atherosclerosis. Circulation 109[suppl III] (2004) III-2-III-7.

[10] M. Gurr, J. Harwood, K. N. Frayn, Lipid Biochemistry. Blackwell Publishing, Malden, MA, 2002.

[11] J. D. Brunzell, A. Chait, E. L. Bierman, Pathophysiology of lipoprotein transport. Metabolism 27 (1978) 1109-1127.

[12] J. L. Goldstein, M. S. Brown, Atherosclerosis: The low-density lipoprotein receptor hypothesis. Metabolism 26 (1977) 1257-1275.

[13] L. Chancharme, P. Therond, F. Nigon, S. Zarev, A. Mallet, et al., LDL particle subclasses in hypercholesterolemia: molecular determinants of reduced lipid hydroperoxide stability. J. Lipid Res. 43 (2002) 453-461.

[14] C. J. Packard, Small dense low density lipoprotein and its role as an independent predictor of cardiovascular disease. Curr. Opin Lipidol. 17 (2006) 412-417.

[15] O. Asrisaka, S. Fujiwara, K. Yabuta., H. Mokuno, Y. Mitugi, et al., Characterization of low-density lipoprotein subclasses in children. Metabolism 46 (1997) 146-148.

[16] S. Alabakovska, D. Labudovic, K. Tosheska, M. Spiroski, B. Todorova, Distribution of low density lipoprotein subclasses in Macedonian children. Med Sci Monit. 10 (2004) CR667-CR671.

[17] P. T. Williams, H. R. Superko, W. L. Haskell, E. L. Alderman, P. J. Blanche, et al., Smallest LDL particles are most strongly related to coronary disease progression in men. Arterioscler Thromb Vasc Biol. 23 (2003) 314-321.

[18] B. A. Griffin, Low density lipoprotein subclasses: mechanisms of formation and modulation. Proc. Nutr. Soc. 56 (1997) 693-702.

[19] M. Rizzo, B. Kaspar, Low-density lipoprotein size and cardiovascular prevention. Eur J Clin Invest. 17 (2005) 77-80.

[20] M. Miyashita, T. Okada, Y. Kuromori, K. Harada, LDL particles size, fat distribution and insulin resistance in obese children. Eur J Clin Nutr. 60 (2005) 416-420.

[21] F. Nigon, Fabienne, P. Lesnik, M. Rouis, M. J. Chapman, Discrete subspecies of human low density lipoproteins are heterogeneous in their interaction with the cellular LDL receptor. J. Lipid Res. 32 (1991) 1741-1753.

[22] K. M. Kostner, G. M. Kostner, Lipoprotein(a): still an enigma? Curr. Opin Lipidol 13 (2002) 391-396.

[23] S. Ishibashi, Lipoprotein (a) and atherosclerosis. Arterioscler Thromb Vasc Biol. 21 (2001) 1-2.

[24] G. Lippi, G. Guidi, Lipoprotein (a): an emerging cardiovascular risk factor. Crit Rev Clin Lab Sci. 40 (2003) 1-42.

[25] I. L. E. Garcia, Differential Density Lipoprotein Profiling for the Characterization of Lipoprotein (a). Ph.D. dissertation, Department of Chemistry, Texas A&M University, College Station, TX (2006).

[26] R. Lawn, Lipoprotein (a) in heart disease. Sci Am 266 (1992) 54-60.

[27] B. Hosken, Density Gradient Ultracentrifugation of Lipoproteins Using Metal Ion Complexes. Ph.D. dissertation, Department of Chemistry, Texas A&M University, College Station, TX (2002).

[28] J. B. Ifft, D. H. Voet, J. Vinograd, The determination of density distributions and density gradients in binary solutions at equilibrium in the ultracentrifuge. J Phys Chem. 65 (1960) 1138-1145.

[29] C. A. Price, Centrifugation in Density Gradients. Academic Press, New York, 1982.

[30] M. K. Brakke, Density gradient centrifugation: a new separation technique. Journal of American Chemical Society. 73 (1951) 1847-1848.

[31] B. D. Hosken, S. L. Cockrill, R. D. Macfarlane. Metal ion complexes of EDTA: a solute system for density gradient ultracentrifugation analysis of lipoproteins. Anal Chem. 77 (2005) 200-207.

[32] J. D. Johnson, N. J. Bell, E. L. Donahow, R. D. Macfarlane, Metal ion complexes of EDTA as solutes for density gradient ultracentrifugation: influence of metal ions. Anal Chem 77 (2005) 7054-7061.

[33] M. Tal, A. Silberstein, E. Nusser, Why does Coomassie brilliant blue R interact differently with different proteins? J. Bio. Chem. 260 (1980) 9976-9980.

[34] M. M. Scalvons, C. M. Cordonnier, P. M. Mailleux, F. R. Heller, J-P. Desageret, et al., Fast separation of the three main plasma lipoprotein classes by ultracentrifugation using vertical rotor and multiple discontinuous density gradient. Clin. Chim. Acta. 153 (1985) 125-135.

[35] D. G. Cornwell, F. A. Kruger, Lipoprotein pre-staining and ultracentrifugal analysis in a density gradient. Proc. Soc. Exptl. Biol. Med. 107 (1961) 296-299.

[36] J. Green, Lipoprotein pre-staining: comparison of nitroblue tetrazolium and sudan black B. Clin Chim Acta. 66 (1976) 295-301.

[37] G. Schmitz, C. Mollers, V. Richter, Analytical capillary isotachophoresis of human serum lipoproteins. Electrophoresis 18 (1997) 1807-1813.

[38] D. P. Via, L.C. Smith, Fluorescent labeling of lipoproteins. Methods Enzymol. 129 (1986) 848-857.

[39] N. G. Lipsky, R. E. Pagano, Sphingolipid metabolism in cultured fibroblasts: microscopic and biochemical studies employing a fluorescent ceramide analogue. Proc. Natl. Acad. Sci. 80 (1983) 2608-2612.

[40] A. Chattopadhyay, Chemistry and biology of N-(7-nitrobenz-2-oxa-1,3-diazol-4-yl)-labeled lipids: fluorescent probes of biological and model membranes. Chem. Phys. Lipids. 53 (1990) 1-15.

[41] B. H. Weiller, L. Ceriotti, T. Shibata, D. Rein, M. Roberts, et al., Analysis of lipoproteins by capillary zone electrophoresis in microfluidic devices: assay development and surface roughness measurements. Anal. Chem. 74 (2002) 1702-1711.

[42] N. Carretti, P. Florio, A. Bertolin, C. V. L. Costa, G. Allegri, et al., Serum fluctuations of total and free tryptophan levels during the menstal cycle are related to gonadotrophins and reflect brain serotonin utilization. Hum Reprod. 20 (2005) 1548-1553.

[43] J. P. Richter (ed.), The Notebooks of Leonardo da Vinci. Dover Publications, Mineola, NY, 1970.

[44] M. Kerker, The Scattering of Light and Other Electromagnetic Radiation. Academic Press, New York, 1969.

[45] H. Gartz, A. Penzkofer, P. Weidner, Nanometer particle size, pore size, and specific surface determination of colloidal suspensions and porous glasses by Rayleigh light scattering. J. Non-Cryst. Solids. 189 (1995) 50-54.

[46] D. M. Pennington, Lasers for Extremely Large Telescopes. Lawrence Livermore National Laboratory. (2003). <http://grus.berkeley.edu/~jrg/LASER/img15.html>.

[47] C. F. Bohren, D. R. Huffman, Absorption and Scattering of Light by Small Particles. John Wiley & Sons, New York, 1983.

[48] A. J. Cox, A. J. DeWeerd, J. Linden, An experiment to measure Mie and Rayleigh total scattering cross sections. Am. J. Phys. 70 (2002) 620-625.

[49] A. Einstein, Investigations on the Theory of Brownian Movement. Dover, New York, 1956.

[50] Malvern Instruments, Dynamic Light Scattering: An Introduction in 30 minutes. Malvern Technical Notes. Vers. MRK656-01. accessed on 4-4-2006 <http://www.malvern.co.uk/malvern/kbase.nsf>.

[51] D. C. Giancoli, Physics: Principles with Applications, 3rd ed. Prentice Hall, Englewood Cliffs, NJ, 1991.

[52] Malvern Instruments, The Accuracy and Precision from DLS measurements." Malvern Technical Notes. Vers. MRK728-01. accessed on 4-4-2006 <http://www.malvern.co.uk/malvern/kbase.nsf>.

[53] Malvern Instruments, Zeta Potential, an Intro in 30 Minutes. Malvern Technical Notes. Vers. MRK654-01. accessed on 4-4-2006 <http://www.malvern.co.uk/malvern/kbase.nsf>.

[54] Ch. –H. Fischer, E. Kenndler, Analysis of colloids IX. Investigation of the electrical double layer of colloidal inorganic nanometer-particles by size-exclusion chromatography. J. Chromattogr. 773 (1997) 179-187.

[55] R. Xu, Shear plane and hydrodynamic diameter of microspheres in suspension. Langmuir 14 (1998) 2593-2597.

[56] D. A. Skoog, D. M. West, F. J. Holler, S. R. Crouch, Analytical Chemistry: An Introduction, seventh edition. Saunders College Publishing, New York, 2000.

[57] W. J. Likos, N. Lu, C. Liverant, Ionic Strength on the Flocculation Behavior of Kaolinite. Colorado School of Mines, Engineering Division, CO, < http://www.ce.utexas.edu/em2000/papers/WLikos.pdf> 2006.

[58] C. Li, G. W. Kattawar, P. Yang, Effects of surface roughness on light scattering by small particles. JQSRT. 89 (2004) 123-131.

[59] R. Hogg, M. L. Turek, E. Kaya, The role of particle shape in size analysis and the evaluation of comminutioin processes. Part. Sci. Technol. 22 (2004) 355-366.

[60] T. Wredt. A review of elastic light scattering theories. Part. Part. Syst. Charact. 15 (1998) 67-74.

[61] R. Antwerpen, Preferred orientations of LDL in vitreous ice indicate a discoid shape of the lipoprotein particle. Arch. Biochem. Biophys. 432 (2004) 122-127.

[62] M. N. Trainer, P. J. Freud, E. M. Leonardo, High-concentration submicron particle size distribution by dynamic light scattering, American Laboratory. 1992. < http://www.microtrac.com/dynamicscattering.cfm#configurations>.

[63] R. L. Davidovich, V. B. Logvinova, T. A. Kaidalova, Antimony(III) ethylenediaminetetraacetate complex compounds with uni- and bicharged cations. Russ J. Coord. Chem. 24 (1998) 399-404.

[64] R. L. Davidovich, A. V. Gerasimenko, V. B. Logvinova, Synthesis and crystal structure of monoprotonated cesium di(ethylenediaminetetraacetato)-dibismuthate(III). Russ J. Inorg. Chem. 46 (2001) 1518-1523.

[65] S. L. Cockrill, Lipoprotein Density Profiling- Assessment of Cardiovascular Risk. Ph.D. dissertation, Department of Chemistry, Texas A&M University, College Station, TX (1998).

[66] M-Y. Liu, C. Mcneal, R. D. Macfarlane, Charge density profiling of circulating human low-density lipoprotein particles by capillary zone electrophoresis. Electrophoresis, 25 (2004) 2985-2995.

[67] D. O'Neal, P. Harrip, G. Dragicevic, D. Rae, J. D. Best, A comparison of LDL size determination using gradient gel electrophoresis and light-scattering methods. J. Lipid Res. 39 (1998) 2086-2090.

[68] S. M. Goldwasser, Diode Pumped Solid State Lasers. Sam's Laser FAQ. 7-01-06. <http://repairfaq.ece.drexel.edu/sam/laserssl.htm#ssldps>.

[69] S. Spiekermann, Compact diode-pumped solid-state lasers. Ph.D. dissertation, Royal Institute of Technology, Stockholm, Sweeden, 2004.

[70] W. F. Krupke, S. A. Payne, C. D. Marshall, Blue diode-pumped solid-state-laser based on ytterbium doped laser crystals operating on the resonance zero-phonon transition. United States Patent, 6,304,584. (2001).

VITA

Michael Nowlin graduated from Coker College in South Carolina in the spring of 2003 with a B.A. in chemistry. In the winter of 2004 he continued his educational endeavors at Texas A&M University where he later joined the Laboratory for Cardiovascular Chemistry headed by Dr. Ronald D. Macfarlane. He defended his research in August of 2006 and received his master's degree in chemistry in December 2006. The author can be contacted at 1006 Hector, Pasadena, TX, 77502.